JEM Journal of Experimental Medicine

ARTICLE

Hepatic stellate and endothelial cells maintain hematopoietic stem cells in the developing liver

Yeojin Lee[1], Juliana Leslie[1], Ying Yang[2], and Lei Ding[1]

The liver maintains hematopoietic stem cells (HSCs) during development. However, it is not clear what cells are the components of the developing liver niche in vivo. Here, we genetically dissected the developing liver niche by systematically determining the cellular source of a key HSC niche factor, stem cell factor (SCF). Most HSCs were closely associated with sinusoidal vasculature. Using *Scf*^{gfp} knockin mice, we found that *Scf* was primarily expressed by endothelial and perisinusoidal hepatic stellate cells. Conditional deletion of *Scf* from hepatocytes, hematopoietic cells, *Ng2*$^{+}$ cells, or endothelial cells did not affect HSC number or function. Deletion of *Scf* from hepatic stellate cells depleted HSCs. Nearly all HSCs were lost when *Scf* was deleted from both endothelial and hepatic stellate cells. The expression of several niche factors was down-regulated in stellate cells around birth, when HSCs egress the developing liver. Thus, hepatic stellate and endothelial cells create perisinusoidal vascular HSC niche in the developing liver by producing SCF.

Introduction

Hematopoietic stem cells (HSCs) rely on niche for their maintenance. In adults, HSCs are sustained by bone marrow perivascular niche composed of multiple cellular components, including endothelial cells (Ding et al., 2012), and mesenchymal stromal cells (Ding and Morrison, 2013; Ding et al., 2012; Greenbaum et al., 2013; Sugiyama et al., 2006), along with other cell types (Morrison and Scadden, 2014). But the bone marrow is not the only organ that supports HSCs. During development, the liver is the major hematopoietic organ in which HSCs expand and mature (Mikkola and Orkin, 2006). It is only after birth that HSCs complete their migration to the bone marrow and reside there throughout adult life (Lee et al., 2017).

In contrast to the adult bone marrow niche, the cellular components of the developing liver niche remain largely undefined in vivo. Stromal cell lines derived from murine fetal liver and fibroblasts derived from human fetal liver can support hematopoiesis in vitro (Hackney et al., 2002; Moore et al., 1997; Tsai et al., 1986). Cells undergoing epithelial-to-mesenchymal transition can also maintain hematopoietic cells in vitro (Chagraoui et al., 2003; Zhang et al., 2005). But the in vivo identities of these cells are not clear. DLK^{+} hepatic progenitors have been shown to express key HSC niche factors and to possess the ability to support HSCs in vitro (Chou and Lodish, 2010). In addition, fetal liver Lyve^{+} endothelial cells can maintain HSCs short-term in vitro (Iwasaki et al., 2010). However, it is not clear whether any of these cells maintain HSCs in vivo. Recently, Nestin^{+}NG2^{+} periportal stromal cells in the fetal liver have been suggested to be an important component of the niche (Khan et al., 2016), as genetic ablation of NG2^{+} cells in a *Ng2-cre*/iDTA mouse model leads to an estimated 30% reduction of phenotypic HSCs. However, fetal liver cells from *Ng2-cre*/iDTA mice have higher reconstituting activity in T and B cell lineages, but not myeloid lineage, compared with littermate controls (Khan et al., 2016), suggesting that functional HSCs are not compromised in these mice. Therefore, there must be other cellular components with critical roles in maintaining HSCs in the developing liver. Overall, it is not clear what cells create a niche for HSCs in the developing liver in vivo.

A niche is defined as the cellular microenvironment that generates necessary cytokines and growth factors for HSC maintenance in vivo. To uncover the HSC niche components in the developing liver, we focused on identification of the cellular sources of key factors required for HSC maintenance in vivo. Stem cell factor (SCF) is one of the very few cytokines known to be genetically required by HSCs. Signaling through the cKIT receptor on HSCs, SCF is essential for HSC maintenance in vivo (Barker, 1994; Ding et al., 2012). *Scf* transcript is alternatively spliced into a short and a long form, with the exclusion or inclusion of an exon containing a proteolytic cleavage site. This leads to two forms of SCF protein, a membrane-bound form and a

[1]Columbia Stem Cell Initiative, Department of Rehabilitation and Regenerative Medicine, Department of Microbiology and Immunology, Columbia University Irving Medical Center, New York, NY; [2]Department of Genetics and Development, Columbia University Irving Medical Center, New York, NY.

Correspondence to Lei Ding: ld2567@cumc.columbia.edu.

soluble form with protease-mediated cleavage (Broudy, 1997). The membrane-bound form of SCF is particularly important for HSC maintenance and implies that its engagement with HSCs is within a local niche (Barker, 1997; Wolf, 1978). *Scf* knockout mice have a profound loss of fetal liver HSCs and are perinatal lethal due to severe hematopoietic defects (Ding et al., 2012; Ikuta and Weissman, 1992). Furthermore, administration of a cKIT functionally blocking antibody during development at times after but not before the liver hematopoietic stages abolishes hematopoietic progenitors, suggesting that the SCF–cKIT pathway is required for HSC maintenance starting from the fetal liver stage (Ogawa et al., 1993). Based on antibody staining, PCR, and a bacterial artificial chromosome transgenic *Scf* reporter allele with likely incomplete promoter, *Scf* has been suggested to be expressed by hepatic progenitors (Azzoni et al., 2018; Chou and Lodish, 2010), Nestin$^+$NG2$^+$ periportal cells (Khan et al., 2016), and endothelial cells (Azzoni et al., 2018). Yet no study has systematically examined which sources of SCF are functionally important for HSCs in the developing liver in vivo. Here, we used Scf^{gfp} knockin and Scf^{fl} conditional knockout mice to systemically characterize the expression of *Scf* and to uncover functionally important cellular sources of SCF for HSC maintenance in the developing liver in vivo. We found that most HSCs localized close to the sinusoidal vasculature, and endothelial and stellate cells are the major functional source of SCF in the perinatal liver. Interestingly, stellate cells down-regulated SCF and several other putative HSC maintenance factors around birth, suggesting that the developing liver is uniquely empowered with HSC-supporting function.

Results

HSCs reside in a perisinusoidal vascular niche in the developing liver

HSCs mature and expand in the fetal liver (Ema and Nakauchi, 2000; Morrison et al., 1995). Around birth, HSCs migrate to and take up residence in the bone marrow (Lee et al., 2017). However, the perinatal time window during which the liver maintains HSCs has not been assessed. We found that liver CD150$^+$CD48$^-$Lin$^-$Sca1$^+$cKit$^+$ HSC frequency and number increased from embryonic day 12.5 (E12.5), peaked at about E15.5, and started to decline from postnatal day 0 (P0; Fig. 1, A and B). By P5, there was a fourfold decrease in fetal liver HSC frequency compared with E15.5. HSCs were essentially undetectable in the liver by P10 (Fig. 1, A and B). To test liver HSC function at these developmental stages, we transplanted 500,000 whole liver cells from E15.5, P0, P5, and P10 mice into lethally irradiated recipient mice along with 500,000 recipient-type bone marrow cells. P0 liver cells had a similar capacity to reconstitute all major hematopoietic lineages (myeloid, B, and T cells) in irradiated mice compared with E15.5 liver cells (Fig. 1 C and Fig. S1 A). The reconstitution potential of P5 liver cells was significantly reduced, although substantial functional HSCs were still present in the liver (Fig. 1 C and Fig. S1 A). P10 liver cells showed a further decline with minimal if any multilineage reconstitution potential (Fig. 1 C and Fig. S1 A). These data suggest that the newborn liver still harbors a functional niche that maintains HSCs. We thus analyzed P0 developing livers throughout our study unless otherwise noted.

We performed SLAM staining on P0 liver sections to localize HSCs in situ and found that CD150$^+$CD48$^-$Lin$^-$ candidate HSCs were closely associated with Laminin$^+$ sinusoidal endothelial cells throughout the liver (Fig. 1, D–H; and Fig. S1, B–E). Similarly, E15.5 fetal liver HSCs were also closely associated with sinusoidal endothelial cells (Fig. S1, F–M). Compared with random mononuclear cells or Lin$^+$CD48$^+$ mature bone marrow cells, HSCs localized significantly closer to sinusoidal endothelial cells (Fig. 1 I). Similar results were obtained when vascular endothelial (VE)–cadherin was used as an endothelial cell marker (Fig. S1, N–S). These data suggest that HSCs localize within a perisinusoidal vascular niche in the developing liver.

Scf is primarily expressed by endothelial cells and hepatic stellate cells

The close association of HSCs to sinusoidal vasculature prompted us to investigate what cells are the source of a key cytokine, SCF, within the perivascular niche. We systematically analyzed *Scf* expression pattern in the developing liver using Scf^{gfp} knockin mice (Ding et al., 2012). Flow-cytometric analyses of enzymatically dissociated P0 $Scf^{gfp/+}$ livers showed that GFP$^+$ cells were rare (~1%) and negative for CD45 and Ter119, markers of hematopoietic cells, indicating that *Scf* is expressed by non-hematopoietic cells (Fig. 2 A and Fig. S2 A). About 83% of CD45$^-$Ter119$^-$CD31$^+$ endothelial cells were positive for GFP, demonstrating that endothelial cells are a source of SCF (Fig. 2 B).

At P0, ~20% of GFP$^+$ stromal cells were CD31$^-$, suggesting that *Scf* is also expressed by stromal cells other than endothelial cells in the developing liver (Fig. 2 C). To elucidate the identity of these cells, we sorted CD45$^-$Ter119$^-$CD31$^-$*Scf*-GFP$^+$ cells by flow cytometry and analyzed their gene expression by quantitative RT-PCR (qRT-PCR). Compared with whole liver, hematopoietic, or CD31$^+$ endothelial cells, CD45$^-$Ter119$^-$CD31$^-$*Scf*-GFP$^+$ cells expressed significantly higher levels of *Desmin*, *Lrat*, *Lhx2*, and *Pdgfrα*, markers of liver-specific perisinusoidal stellate cells (Mederacke et al., 2013; Tsutsumi et al., 1987; Wandzioch et al., 2004; Wright et al., 2014; Yin et al., 2013; Fig. 2 D), suggesting that these *Scf*-GFP$^+$ cells are hepatic stellate cells. *Cxcl12*, a chemokine required for HSC maintenance and homing (Ara et al., 2003; Ding and Morrison, 2013; Greenbaum et al., 2013; Sugiyama et al., 2006), was also highly expressed by the non-endothelial CD45$^-$Ter119$^-$CD31$^-$*Scf*-GFP$^+$ cells (Fig. 2 D). It has been reported that fetal liver stellate cells express *Cxcl12* (Kubota et al., 2007). Consistently, using $Cxcl12^{DsRed/+}$ knockin reporter mice (Ding and Morrison, 2013), we found that virtually all (95%) *Cxcl12*-DsRed$^+$ cells were Desmin$^+$ in P0 livers (Fig. 2, E–J). CD45$^-$Ter119$^-$*Cxcl12*-DsRed$^+$ stromal cells from P0 livers of $Cxcl12^{DsRed/+}$ mice consistently expressed significantly higher levels of *Desmin*, *Lrat*, *Lhx2*, and *Pdgfrα* compared with whole liver cells (Fig. S2 B). We systematically examined the expression of *Cxcl12* in P0 livers and found that *Cxcl12* was not expressed by hematopoietic, hepatic, or CD31$^+$ endothelial cells (Fig. S2, C and D). Mature hepatic stellate cells have the unique characteristic of storing vitamin A in their cytoplasm

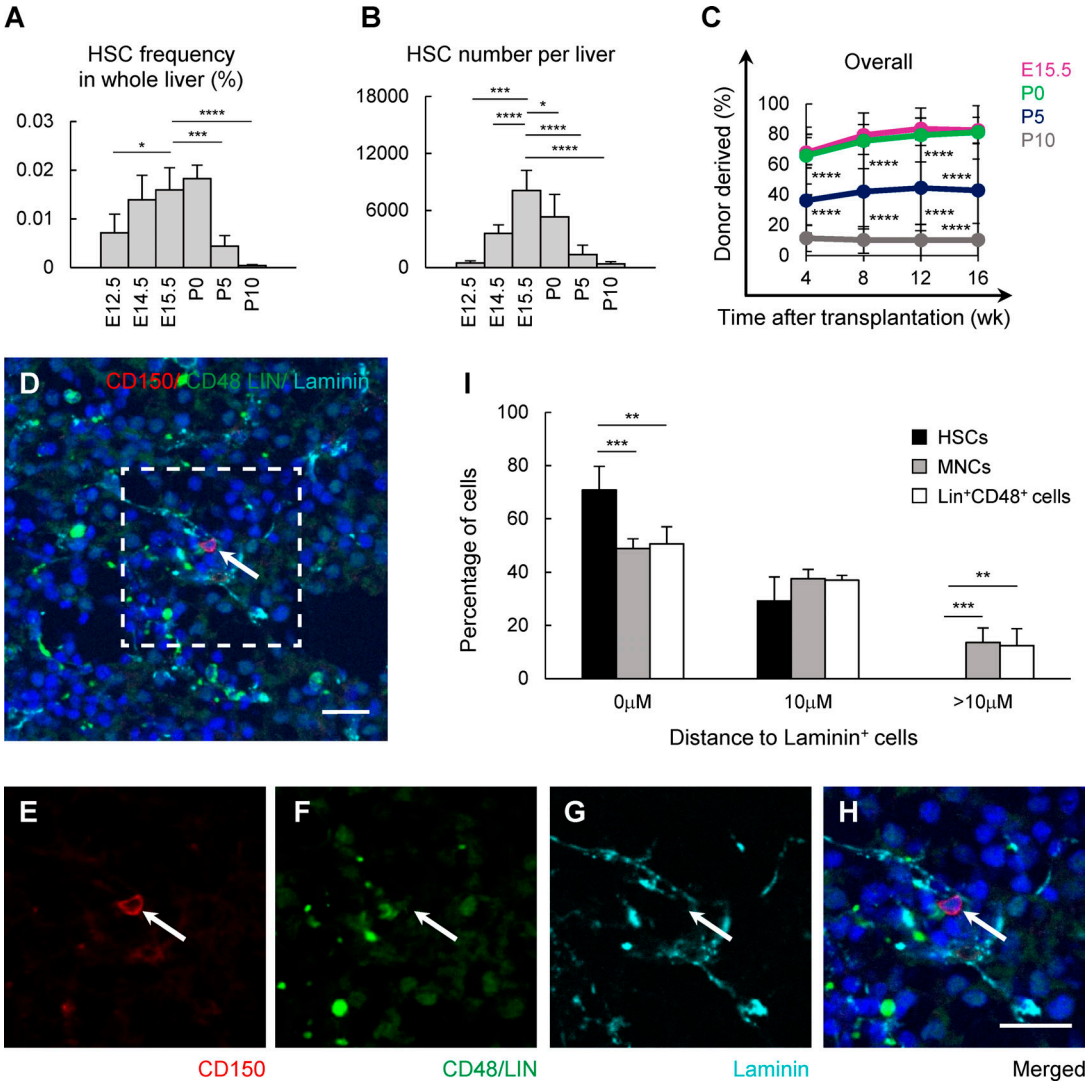

Figure 1. **HSCs localize in perisinusoidal niche of the developing liver. (A)** HSC frequency from E12.5, E14.5, E15.5, P0, P5, and P10 livers analyzed by flow cytometry (n = 3 embryos for E12.5, n = 4 embryos for E14.5, n = 8 embryos for E15.5, n = 14 mice for P0, n = 5 mice for P5, and n = 4 mice for P10). **(B)** HSC number from E12.5, E14.5, E15.5, P0, P5, and P10 livers (n = 3 embryos for E12.5, n = 4 embryos for E14.5, n = 7 embryos for E15.5, n = 14 mice for P0, n = 5 mice for P5, and n = 4 mice for P10). **(C)** Long-term multilineage reconstitution assays. Irradiated recipient mice ($CD45.1^+$) were transplanted with 5×10^5 liver cells from E15.5, P0, P5, or P10 donor ($CD45.2^+$) mice together with 5×10^5 recipient ($CD45.1^+$) bone marrow cells (n = 4 recipient mice for E15.5, n = 62 recipient mice for P0, n = 11 recipient mice for P5, and n = 20 recipient mice for P10). **(D–H)** A $CD150^+CD48^-Lin^-$ candidate HSC localized adjacent to sinusoidal endothelial cells in the P0 liver. Endothelial cells were stained with an anti-Laminin antibody. Nuclei were stained with DAPI, in blue. E–H are insets of the selected area in D. **(I)** Distribution of distances between $Laminin^+$ endothelial cells and $CD150^+CD48^-Lin^-$ candidate HSCs, random mononuclear cells (MNCs; n = 3,059), or Lin^+CD48^+ cells (n = 372). $DAPI^+$ cells were defined as random mononuclear cells. Measurements for all images were performed using ImageJ software. A total of 40 HSCs were quantified from three independent experiments. All data represent mean ± SD. Two-tailed Student's t tests were used to evaluate statistical significance. *, P < 0.05; **, P < 0.01; ***, P < 0.001; ****, P < 0.0001. Scale bars are 20 μm in D and H.

(Mederacke et al., 2013). Indeed, the majority of $CD45^-Ter119^-$*Cxcl12*-$DsRed^+$ stromal cells were vitamin A^+ by flow cytometry analysis (Fig. 2 K). Taken together, our data established *Cxcl12*-DsRed as a specific marker for hepatic stellate cells in the developing liver.

We generated $Scf^{gfp/+}$; $Cxcl12^{DsRed/+}$ mice to directly test whether hepatic stellate cells are indeed a cellular source of SCF in the developing liver. By flow cytometry, ∼78% of $CD45^-Ter119^-$*Cxcl12*-$DsRed^+$ stellate cells were *Scf*-GFP^+ (Fig. 2 L). $Cxcl12^+$ stellate cells accounted for the majority (81%) of nonendothelial $CD45^-Ter119^-CD31^-$*Scf*-GFP^+ cells (Fig. 2 M). Thus, besides endothelial cells, stellate cells are a major source of SCF in the developing liver.

qRT-PCR analyses revealed that endothelial cells and hepatic stellate cells expressed *Scf* at ∼155-fold and ∼50-fold the levels found in whole P0 liver cells, respectively (Fig. 2 N). Consistent with our flow cytometry data (Fig. 2 A and Fig. S2 A), hematopoietic cells and hepatocytes expressed very little if any *Scf* (Fig. 2 N). $Ng2^+$ cells expressed an ∼12-fold higher level of *Scf* compared with whole liver cells (Fig. 2 N). The short (membrane-bound) and long (with the potential to become soluble) forms of *Scf* showed similar expression patterns in endothelial

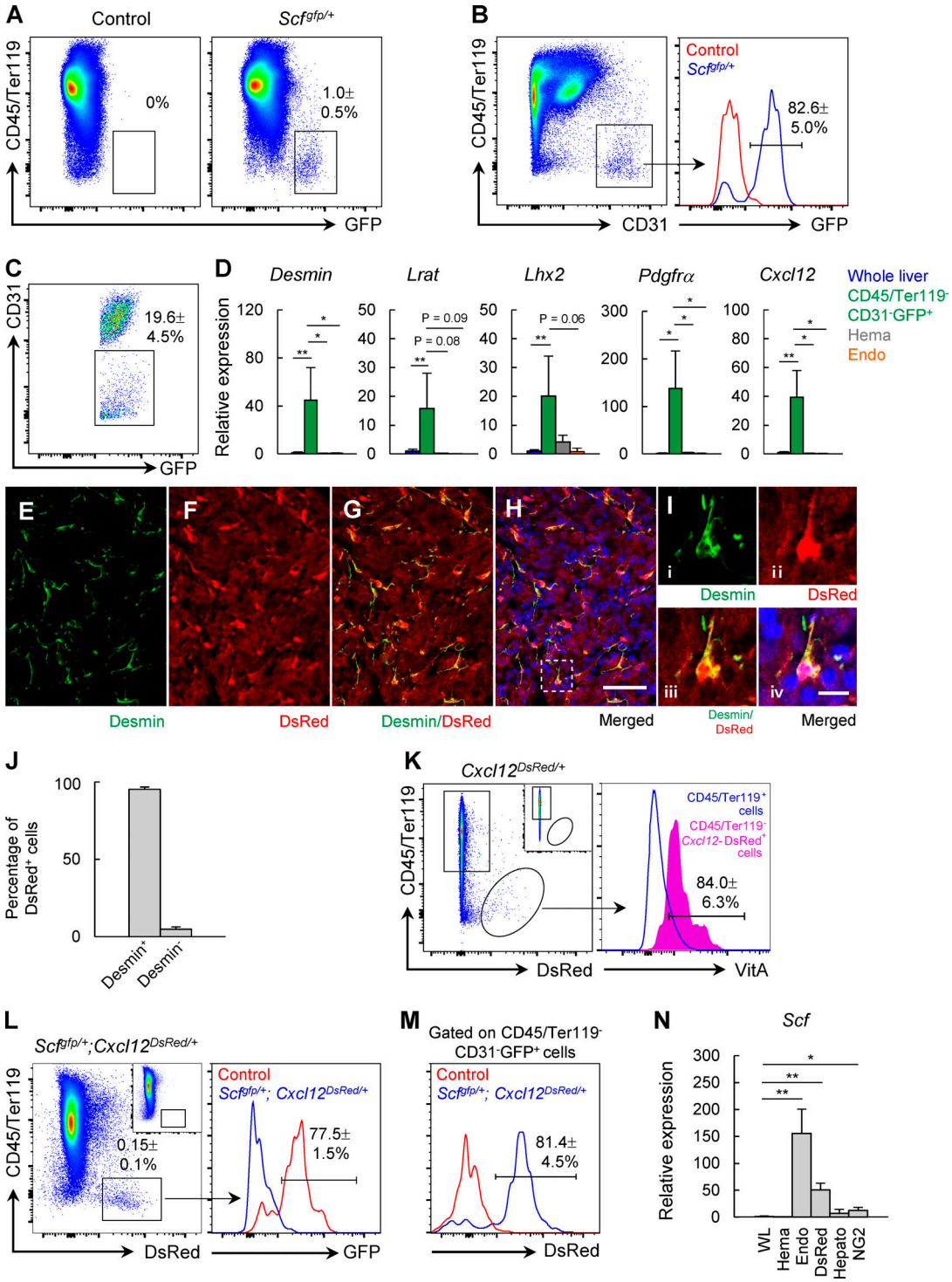

Figure 2. **Endothelial cells and hepatic stellate cells are the major sources of SCF in the developing liver. (A)** *Scf*-GFP was expressed by rare CD45$^-$Ter119$^-$ nonhematopoietic cells in the P0 liver (n = 7 mice for control, and n = 13 mice for *Scf*$^{gfp/+}$). **(B)** The majority of CD45$^-$Ter119$^-$CD31$^+$ endothelial cells in the P0 liver expressed *Scf*-GFP (n = 5 mice for control, and n = 12 mice for *Scf*$^{gfp/+}$). **(C)** *Scf*-GFP was also expressed by CD31$^-$ nonendothelial stromal cells (n = 13 mice for *Scf*$^{gfp/+}$). CD45$^-$Ter119$^-$*Scf*-GFP$^+$ cells are shown. **(D)** qRT-PCR revealed that CD45$^-$Ter119$^-$CD31$^-$*Scf*-GFP$^+$ cells had significantly higher expression of *Desmin*, *Lrat*, *Lhx2*, *Pdgfrα*, and *Cxcl12* compared with P0 whole liver cells [WL], hematopoietic cells, or endothelial cells (n = 5 for whole liver cells, n = 4 for CD45$^-$Ter119$^-$CD31$^-$*Scf*-GFP$^+$ cells, n = 3 for CD45$^+$ or Ter119$^+$ hematopoietic cells [Hema], and n = 3 for CD45$^-$Ter119$^-$CD31$^+$ endothelial cells [Endo]). **(E–I)** *Cxcl12*-DsRed was expressed by Desmin$^+$ cells in the P0 liver. Nuclei were stained with DAPI, in blue. I is an inset of the selected area in H. Roman numerals i–iv indicate individual channels and merged images. **(J)** Quantification of DsRed$^+$Desmin$^+$ cells and DsRed$^+$Desmin$^-$ cells from *Cxcl12*$^{DsRed/+}$ P0 liver tissue sections. About 98% of DsRed$^+$ cells were Desmin$^+$. Three representative confocal images from two independent experiments were used for quantification. **(K)** The majority of P0 liver CD45$^-$Ter119$^-$*Cxcl12*-DsRed$^+$ stromal cells were vitamin A$^+$ (VitA; n = 5 mice for *Cxcl12*$^{DsRed/+}$). **(L)** The majority of P0 liver CD45$^-$Ter119$^-$*Cxcl12*-DsRed$^+$ stellate cells expressed *Scf*-GFP in *Scf*$^{gfp/+}$; *Cxcl12*$^{DsRed/+}$ mice (n = 4 mice for control, and n = 7 mice for *Scf*$^{gfp/+}$; *Cxcl12*$^{DsRed/+}$).

(M) The majority of P0 liver CD45⁻Ter119⁻CD31⁻*Scf*-GFP⁺ stromal cells were *Cxcl12*-DsRed⁺ (n = 3 mice for control, and n = 7 mice for $Scf^{gfp/+}$; $Cxcl12^{DsRed/+}$). **(N)** *Scf* transcript levels in distinct cell populations of P0 liver as quantified by qRT-PCR (n = 3 for WL, n = 3 for Hema, n = 3 for Endo, n = 3 for CD45⁻Ter119⁻*Cxcl12*-DsRed⁺ stellate cells [DsRed], n = 4 for CD45⁻Ter119⁻tdTomato⁺ hepatocyte lineage cells from *Albumin-cre; loxp-tdTomato* mice [Hepato], and n = 3 for NG2⁺). All data represent mean ± SD. Two-tailed Student's t tests were used to evaluate statistical significance. *, P < 0.05; **, P < 0.01. Scale bars are 50 µm in H and 10 µm in I.

and stellate cells (Fig. S2 E). Endothelial and stellate cells were also the major source of *Scf* in E15.5 fetal livers, although at this stage, stellate cells expressed *Scf* at a higher level than endothelial cells (Fig. S2, F–O). Throughout development, stellate cells gradually mature with up-regulated expression of *Desmin* and *Lrat*, and accumulation of vitamin A (Fig. S2, P and Q). Taken together, these data suggest that endothelial cells and hepatic stellate cells are the major sources of SCF in the developing liver.

CD150⁺CD48⁻Lin⁻ HSCs were closely associated with Desmin⁺ perisinusoidal stellate cells (Fig. S3, A–F). This raised the possibility that HSCs reside in a perisinusoidal vascular niche composed of endothelial cells and hepatic stellate cells in the developing liver.

HSCs do not require SCF from hepatic cells in the developing liver

To test which cells are the functionally important sources of SCF for HSC maintenance in the developing liver in vivo, we systematically deleted *Scf* from candidate niche cells. Hepatic lineage cells have been proposed to be a candidate niche cell type for fetal liver HSCs (Chou and Lodish, 2010). But it is not clear whether hepatocytes are a source of SCF for developing liver HSC maintenance in vivo. *Albumin-cre* effectively recombines genes in fetal and postnatal hepatocytes (Weisend et al., 2009). Consistent with this, we found that *Albumin-cre* recombined a *loxp-tdTomato*⁺ reporter in HNF4α⁺ hepatic cells of P0 livers efficiently (Fig. 3, A–E). To test whether hepatocytes are an important source of SCF for HSC maintenance in the developing liver, we generated and analyzed newborn *Albumin-cre;* $Scf^{fl/-}$ mice. P0 livers from $Scf^{+/-}$ germline heterozygous mice exhibited a normal HSC frequency but an approximately twofold decline in cellularity compared with WT controls (Fig. 3, F and G). No discernable morphological abnormalities were observed in the P0 livers from $Scf^{+/-}$ mice, suggesting that the decrease in cellularity is largely due to loss of hematopoietic cells (Fig. S3, G–V). Deletion of *Scf* from hepatic cells in *Albumin-cre;* $Scf^{fl/-}$ mice did not significantly reduce HSC frequency in the developing liver compared with either WT or germline $Scf^{+/-}$ heterozygous mice (Fig. 3 F). Compared with $Scf^{+/-}$ heterozygous mice, deletion of the second allele of *Scf* from hepatic cells in *Albumin-cre;* $Scf^{fl/-}$ mice did not lead to a further loss of liver cellularity or HSC number (Fig. 3, G and H). To determine whether functional HSCs were impaired in the developing livers of *Albumin-cre;* $Scf^{fl/-}$ mice, we transplanted 500,000 P0 liver cells from *Albumin-cre;* $Scf^{fl/-}$, littermate $Scf^{+/+}$, or $Scf^{+/-}$ mice along with 500,000 recipient-type bone marrow cells into lethally irradiated recipient mice. Consistent with the normal HSC frequency in $Scf^{+/-}$ livers (Fig. 3 F), 500,000 P0 liver cells from $Scf^{+/+}$ and $Scf^{+/-}$ mice gave similar reconstitution (Fig. S3 W). Thus, hereafter throughout this study, reconstitution data from liver cells of $Scf^{+/+}$ and/or $Scf^{+/-}$ mice were combined as controls unless otherwise noted. Importantly, P0 liver cells from *Albumin-cre;* $Scf^{fl/-}$ mice had normal reconstitution activity compared with controls (Fig. 3 I). These data demonstrate that *Scf* from hepatocytes is not required for HSC maintenance in the developing liver in vivo.

HSCs do not require SCF from hematopoietic cells in the developing liver

Although hematopoietic cells express very little if any *Scf* (Fig. 2, A and N; and Fig. S2 A), it was still possible that hematopoietic cells are an important functional source of SCF for HSC maintenance in the developing liver. We thus conditionally deleted *Scf* from hematopoietic cells using *Vav1-cre* (de Boer et al., 2003). Consistent with prior reports (de Boer et al., 2003; Ding et al., 2012), recombination was highly efficient in HSCs and other hematopoietic cells from *Vav1-cre;* $Scf^{fl/-}$ P0 livers (Fig. 4, A and B). *Vav1-cre;* $Scf^{fl/-}$ mice had normal HSC frequency in the P0 livers relative to WT or germline $Scf^{+/-}$ heterozygous littermate control mice (Fig. 4 C). Compared with $Scf^{+/-}$ mice, *Vav1-cre;* $Scf^{fl/-}$ mice had similar cellularity and HSC numbers in the P0 livers (Fig. 4, D and E). P0 liver cells from *Vav1-cre;* $Scf^{fl/-}$ mice had normal reconstitution capacity in all major blood lineages (Fig. 4 F). Therefore, *Scf* expressed by hematopoietic cells is not required for HSC maintenance in the developing liver.

HSCs do not require SCF from *Ng2*⁺ cells in the developing liver

Ng2⁺ periportal stromal cells have been proposed to be a component of the fetal liver niche (Khan et al., 2016). Consistent with the prior report, we found that *Ng2-cre* recombined in α-SMA⁺ periportal stromal cells in the developing liver (Fig. 5, A–E). Deletion of *Scf* from periportal stromal cells in *Ng2-cre;* $Scf^{fl/-}$ mice did not significantly reduce HSC frequency in the developing liver (Fig. 5 F). P0 liver cellularity and HSC number did not significantly differ in *Ng2-cre;* $Scf^{fl/-}$ mutants compared with littermate $Scf^{+/-}$ controls (Fig. 5, G and H). Moreover, P0 liver cells from *Ng2-cre;* $Scf^{fl/-}$ mice had normal long-term myeloid and T cell reconstituting activity and a slight increase in B cell lineage reconstitution compared with controls (Fig. 5 I), consistent with a lack of hematopoietic reconstitution defects when *Ng2*⁺ cells are genetically ablated (Khan et al., 2016). These data demonstrate that *Scf* from *Ng2-cre*⁺ cells do not contribute to HSC maintenance in the developing liver.

Deletion of *Scf* from endothelial cells does not cause significant HSC depletion

Tie2-cre recombines in endothelial and hematopoietic cells (Ding et al., 2012; Kisanuki et al., 2001). We generated *Tie2-cre;* $Scf^{fl/-}$ mice to conditionally delete *Scf* from these cells. Since hematopoietic cells do not express *Scf* (Fig. 2, A and N; and Fig. S2 A) and *Scf* from hematopoietic cells is not required for HSC maintenance in the developing liver (Fig. 4), this model allowed us to

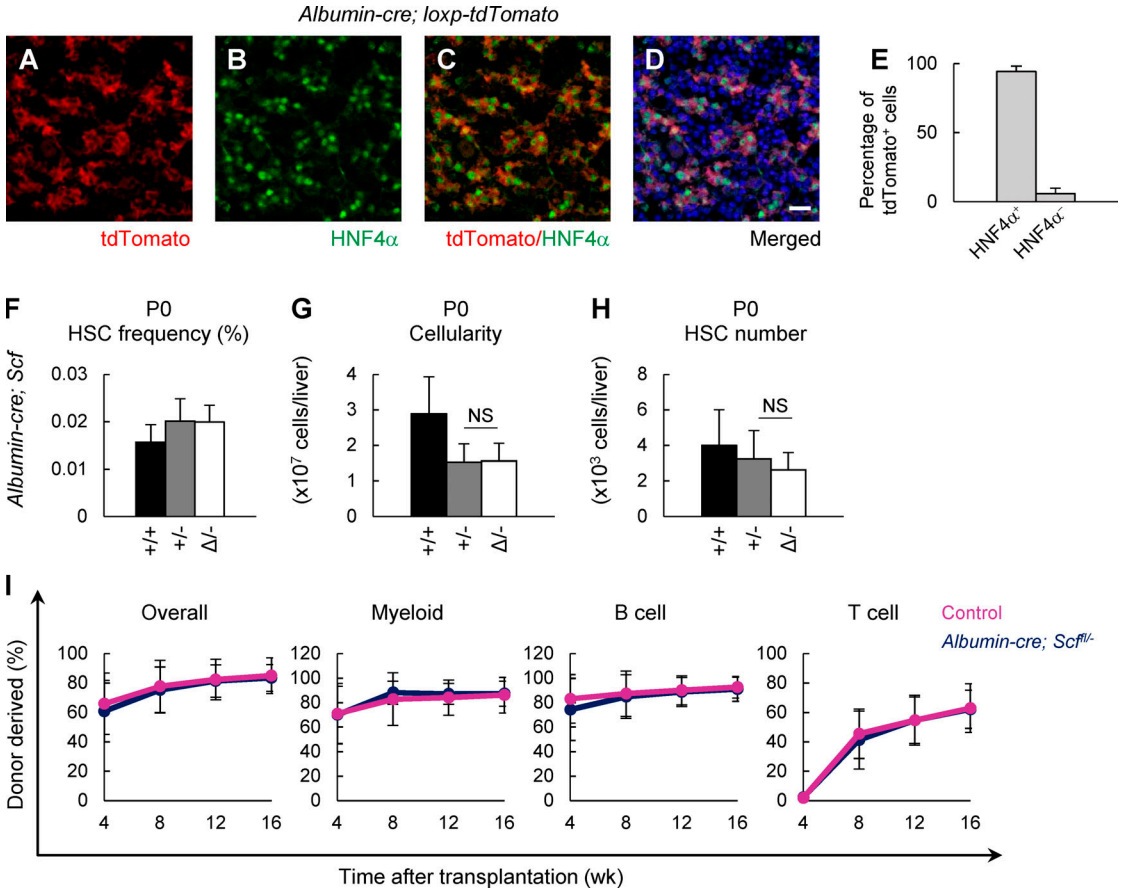

Figure 3. ***Scf* from hepatocytes is not required for HSC maintenance in the developing liver. (A–D)** Representative confocal images showing that virtually all hepatocytes were tdTomato⁺ in *Albumin-cre; loxp-tdTomato* P0 mice. Hepatocytes were stained with an anti-HNF4α antibody. Nuclei were stained with DAPI, in blue. **(E)** Quantification of *tdTomato*⁺ cells in P0 *Albumin-cre; loxp-tdTomato* mice. The numbers of tdTomato⁺HNF4α⁺ cells and tdTomato⁺HNF4α⁻ cells were counted from three independent confocal images. **(F–H)** HSC frequency (F), liver cellularity (G), and HSC number (H) in P0 *Albumin-cre; Scf*$^{fl/-}$ mice compared with littermate controls (n = 5 mice for *Scf*$^{+/+}$, n = 4 mice for *Scf*$^{+/-}$, and n = 7 mice for *Albumin-cre; Scf*$^{fl/-}$). **(I)** 5 × 10^5 P0 liver cells from *Albumin-cre; SScf*$^{fl/-}$ mice gave normal levels of reconstitution in irradiated mice (data represent three independent experiments with a total of n = 24 recipients for controls and n = 15 recipients for mutants). *Scf*$^{+/+}$ and *Scf*$^{+/-}$ mice were used as controls. +, WT allele; Δ, recombined *Scf*^{fl} allele; –, germline deleted allele. *Scf*$^{+/+}$ mice include *Cre; Scf*$^{+/+}$ and *Cre; Scf*$^{fl/+}$ mice. *Scf*$^{+/-}$ mice include *Cre*(–); *Scf*$^{+/-}$ and *Cre*(–); *Scf*$^{fl/-}$ mice. All data represent mean ± SD. Two-tailed Student's *t* tests were used to evaluate statistical significance.

investigate whether endothelial cells are a critical source of SCF for HSC maintenance. As expected, *Tie2-cre* efficiently recombined in *Scf*-expressing CD31⁺ endothelial cells in P0 livers (Fig. 6, A and B). *Tie2-cre; Scf*$^{fl/-}$ mutants had normal HSC frequency compared with littermate controls in the developing liver (Fig. 6 C). Liver cellularity and the number of HSCs in the developing livers of *Tie2-cre; Scf*$^{fl/-}$ mutants did not differ significantly from littermate *Scf*$^{+/-}$ controls (Fig. 6, D and E). Competitive reconstitution assays revealed that P0 liver cells from *Tie2-cre; Scf*$^{fl/-}$ mice had normal reconstitution capacity compared with controls (Fig. 6 F). Thus, deletion of *Scf* from endothelial cells alone does not significantly affect either the number or the function of HSCs in the developing liver.

Deletion of *Scf* from hepatic stellate cells leads to loss of HSCs in the developing liver

We found that *Pdgfrα*, a mesenchymal cell marker (Andrae et al., 2008; Li et al., 2018), was highly expressed by CD45⁻Ter119⁻*Cxcl12*-DsRed⁺ hepatic stellate cells in the developing liver (Fig. 2 D and Fig. S2 B), raising the possibility that we could conditionally delete *Scf* from stellate cells using a *Pdgfrα-cre* transgenic line (Roesch et al., 2008). We generated *Pdgfrα-cre; loxp-tdTomato* mice to examine its recombination pattern in the developing liver. About 90% of tdTomato⁺ cells were Desmin⁺ stellate cells (Fig. 7, A–E), with minimal if any recombination in endothelial cells (0%), hematopoietic cells (0.3%), or hepatocytes (0.6%; Fig. S4, A–J). A minimal number of α-SMA⁺ cells (5%) were targeted by *Pdgfrα-cre* in P0 livers (Fig. S4, K–O). Thus, the *Pdgfrα-cre* transgenic line recombines specifically and efficiently in perisinusoidal stellate cells in the developing liver.

To test whether *Pdgfrα-cre*–expressing stellate cells are an important source of SCF for HSC maintenance, we generated *Pdgfrα-cre; Scf*$^{fl/fl}$ and *Pdgfrα-cre; Scf*$^{fl/-}$ mice. These mice had normal HSC frequency in the developing liver compared with controls (Fig. 7 F). However, liver cellularity as well as HSC number in the P0 livers from *Pdgfrα-cre; Scf*$^{fl/fl}$ or *Pdgfrα-cre; Scf*$^{fl/-}$ mice were significantly reduced compared with either *Scf*$^{+/+}$ or *Scf*$^{+/-}$ littermate controls (Fig. 7, G and H). Importantly, 500,000 P0 liver cells from

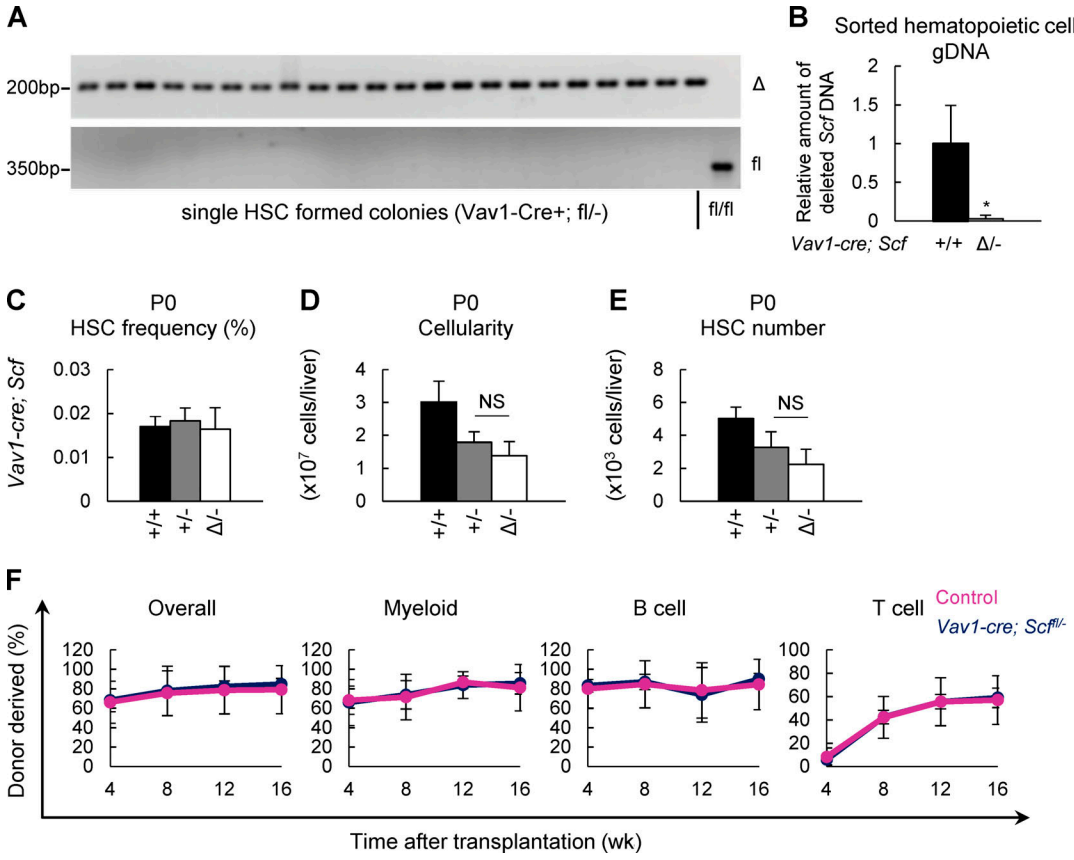

Figure 4. ***Scf* from hematopoietic cells is not required for HSC maintenance in the developing liver. (A)** Genotyping of individual colonies formed by single HSCs isolated from *Vav1-cre; Scf*$^{fl/-}$ mice. *Vav1*-Cre recombined the *Scf*^{fl} allele in all 22 colonies. **(B)** Quantification of recombined *Scf*^{fl} allele in CD45$^+$ and/or Ter119$^+$ hematopoietic cells purified from control (*Scf*$^{fl/fl}$) or *Vav1-cre; Scf*$^{fl/-}$ mice by qPCR (n = 3 mice for control, n = 3 mice for *Vav1-cre; Scf*$^{fl/-}$). gDNA, genomic DNA. **(C–E)** HSC frequency (C), cellularity (D), and HSC number (E) in P0 livers from *Vav1-cre; Scf*$^{fl/-}$ mice compared with littermate controls (n = 6 mice for *Scf*$^{+/+}$, n = 4 mice for *Scf*$^{+/-}$, and n = 7 mice for *Vav1-cre; Scf*$^{fl/-}$). **(F)** 5 × 10^5 liver cells from *Vav1-cre; Scf*$^{fl/-}$ mice gave normal levels of reconstitution in irradiated mice (data represent three independent experiments with a total of n = 14 recipients per genotype). *Scf*$^{+/+}$ and *Scf*$^{+/-}$ mice were used as controls. +, WT allele; Δ, recombined *Scf*^{fl} allele; –, germline deleted allele. *Scf*$^{+/+}$ mice include *Cre; Scf*$^{+/+}$, *Cre; Scf*$^{fl/+}$, *Cre*(–); *Scf*$^{fl/+}$, and *Cre*(–); *Scf*$^{fl/fl}$ mice. *Scf*$^{+/-}$ mice include *Cre; Scf*$^{+/-}$, *Cre*(–); *Scf*$^{+/-}$, and *Cre*(–); *Scf*$^{fl/-}$ mice. All data represent mean ± SD. Two-tailed Student's t tests were used to evaluate statistical significance. *, $P < 0.05$.

Pdgfrα-cre; Scf$^{fl/fl}$ or *Pdgfrα-cre; Scf*$^{fl/-}$ mice gave modest but significantly lower levels of reconstitution compared with controls when transplanted into lethally irradiated recipient mice (Fig. 7 I). We also analyzed these mice at E15.5 and did not observe significant decreases in liver cellularity or HSC number compared with *Scf*$^{+/-}$ littermate controls (Fig. S5, A–C). E15.5 liver cells from these mutant mice had normal long-term multilineage reconstitution activity (Fig. S5 D), suggesting that the depletion of HSCs in P0 livers (Fig. 7, F–I) was not due to developmental defects before E15.5. These data suggest that HSC niche in the mutant mice was functionally compromised in the developing liver. We also analyzed these mice at P5, when the liver still contains a substantial number of HSCs (Fig. 1, A–C). Compared with controls, *Pdgfrα-cre; Scf*$^{fl/fl}$ or *Pdgfrα-cre; Scf*$^{fl/-}$ mice had a significant decrease of HSC frequency (Fig. 7 J). Liver HSC number was markedly depleted at P5 (Fig. 7, K and L). These data suggest that HSCs are progressively depleted in the developing livers of *Pdgfrα-cre; Scf*$^{fl/fl}$ or *Pdgfrα-cre; Scf*$^{fl/-}$ mice.

Compared with littermate controls, P5 *Pdgfrα-cre; Scf*$^{fl/fl}$ mice were smaller in size, with smaller and pale spleens and livers (Fig. 7, M–O) and significant decreases in white blood cell, red blood cell, and platelet counts in the peripheral blood (Fig. S5, E–G). By P10, *Pdgfrα-cre; Scf*$^{fl/fl}$ mice had severe growth retardation with small spleens and livers (Fig. S5, H–J). The vast majority of the *Pdgfrα-cre; Scf*$^{fl/fl}$ mice (14 out of 15 mutants from 11 independent litters) died before the weaning age (P21), while none of the controls did so (Fig. S5 K). The preweaning death of *Pdgfrα-cre; Scf*$^{fl/fl}$ mice could be rescued by transplantation of WT bone marrow cells (four out of four mutants survived to adulthood after the bone marrow transplantation; Fig. S5 L), suggesting that these mice died of hematopoietic failure. Taken together, our data demonstrate that loss of *Scf* from hepatic stellate cells leads to loss of HSCs in the developing liver and early postnatal lethality due to hematopoietic defects.

HSCs require SCF from both endothelial and hepatic stellate cells

Both endothelial and hepatic stellate cells are the major source of SCF in the developing liver (Fig. 2 and Fig. S2). However, deletion of *Scf* from endothelial cells did not result in significant HSC depletion (Fig. 6, C–F), while deletion of *Scf* from stellate cells

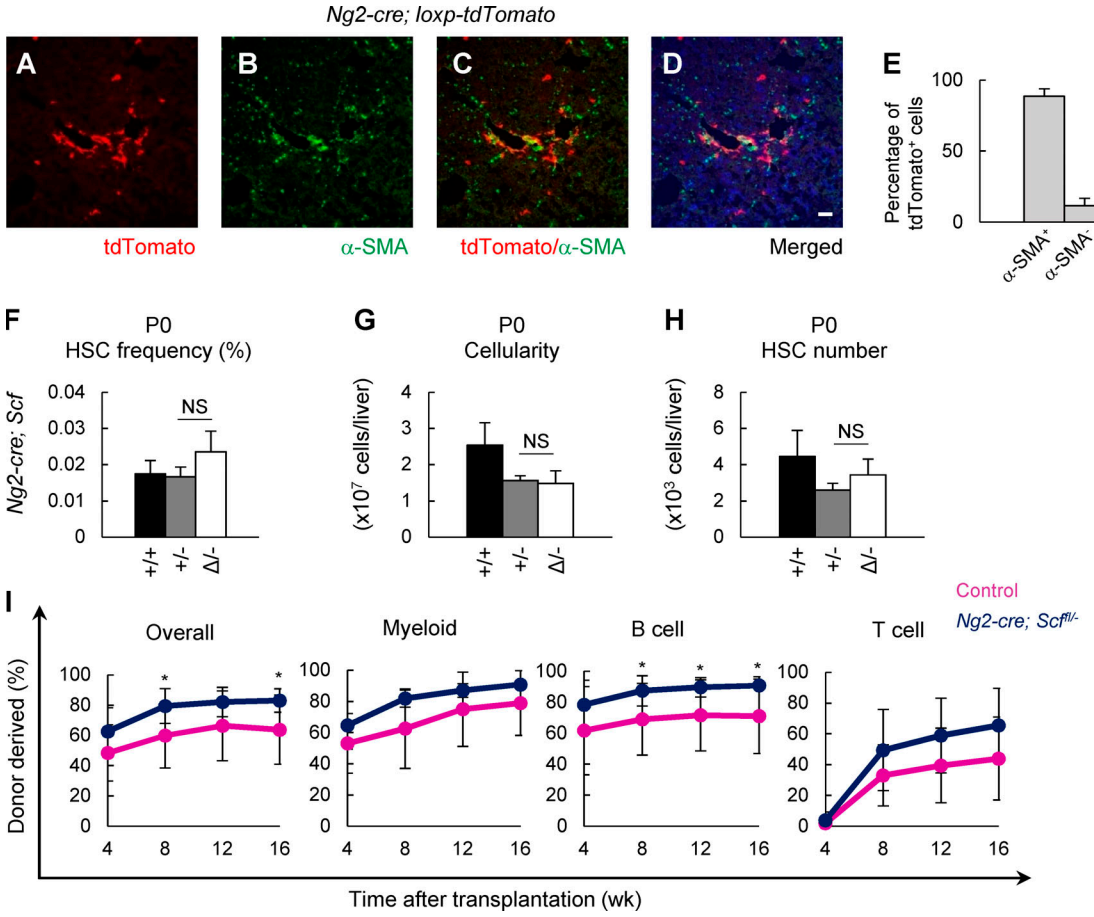

Figure 5. ***Scf* from *Ng2*⁺ cells is not required for HSC maintenance in the developing liver. (A–D)** Representative confocal immunofluorescence images of *Ng2-cre; loxp-tdTomato* P0 liver sections. *Ng2*-cre recombined in α-SMA⁺ periportal stromal cells in the P0 liver. *Ng2*⁺ periportal stromal cells were stained with an anti-α-SMA antibody. Nuclei were stained with DAPI, in blue. **(E)** Quantification of tdTomato⁺α-SMA⁺ cells and tdTomato⁺α-SMA⁻ cells from confocal images of *Ng2-cre; loxp-tdTomato* P0 liver tissue sections. The quantification was from three independent confocal images. **(F–H)** HSC frequency (F), liver cellularity (G), and HSC number (H) in P0 *Ng2-cre; Scf*$^{fl/-}$ mice and littermate controls (n = 9 mice for *Scf*$^{+/+}$, n = 4 mice for *Scf*$^{+/-}$, and n = 10 mice for *Ng2-cre; Scf*$^{fl/-}$). **(I)** 5 × 10^5 liver cells from *Ng2-cre; Scf*$^{fl/-}$ mice gave normal levels of reconstitution in irradiated mice, except an elevated level contribution to B cell lineage, relative to controls (data represent two independent experiments with a total of n = 8 recipients for controls and n = 9 recipients for mutants). *Scf*$^{+/+}$ and *Scf*$^{+/-}$ mice were used as controls. +, WT allele; Δ, recombined *Scf*^{fl} allele; –, germline deleted allele. *Scf*$^{+/+}$ mice include *Cre; Scf*$^{fl/+}$, *Cre*(–); *Scf*$^{fl/+}$, and *Cre*(–); *Scf*$^{fl/fl}$ mice. *Scf*$^{+/-}$ mice include *Cre*(–); *Scf*$^{fl/-}$ mice. All data represent mean ± SD. Two-tailed Student's t tests were used to evaluate statistical significance. *, P < 0.05. Scale bar is 50 µm in D.

resulted in only modest reconstitution defects (Fig. 7 I). This raised the question of whether SCF from endothelial and hepatic stellate cells synergistically maintains HSCs in the developing liver. To directly test this, we generated *Pdgfrα-cre; Tie2-cre; Scf*$^{fl/-}$ mice.

Pdgfrα-cre; Tie2-cre; Scf$^{fl/-}$ mice were born smaller with pale livers, suggesting a hematopoietic defect in the liver (Fig. 8, A and B). P0 livers from *Pdgfrα-cre; Tie2-cre; Scf*$^{fl/-}$ mice had significant decreases in HSC frequency, cellularity, and HSC number compared with controls (Fig. 8, C–E). P0 liver cells from *Pdgfrα-cre; Tie2-cre; Scf*$^{fl/-}$ mice had a significantly reduced capacity to reconstitute lethally irradiated recipient mice in competitive reconstitution assays (Fig. 8 F), with significantly lower contribution to bone marrow HSCs and Lin⁻Sca1⁺cKit⁺ (LSK) progenitors in the recipient mice compared with controls (Fig. 8 G). The hematopoietic defects of the mutant mice became more prominent at P5 (Fig. 8, H and I). Strikingly, ∼90% of HSCs were depleted from the P5 livers of *Pdgfrα-cre; Tie2-cre; Scf*$^{fl/-}$ mice (Fig. 8, J–L). Importantly, multilineage reconstitution activity was largely depleted from P5 liver cells of *Pdgfrα-cre; Tie2-cre; Scf*$^{fl/-}$ mice upon transplantation, with mutant liver cells contributing significantly lower levels of HSCs and LSK progenitors in the recipients (Fig. 8, M and N). These data suggest that endothelial and stellate cells are the major source of SCF in the developing liver.

At E14.5, livers from *Pdgfrα-cre; Tie2-cre; Scf*$^{fl/-}$ mice had normal HSC frequency, cellularity, and HSC numbers compared with *Scf*$^{+/-}$ heterozygous mice (Fig. S5, M–O). Notably, E14.5 liver cells from *Pdgfrα-cre; Tie2-cre; Scf*$^{fl/-}$ mice had normal reconstitution capacity (Fig. S5 P). These data suggest that the HSC depletion observed in the P0 developing livers from *Pdgfrα-cre; Tie2-cre; Scf*$^{fl/-}$ mice (Fig. 8) does not reflect developmental defects before E14.5. Taken together, these data strongly suggest that endothelial cells cooperate

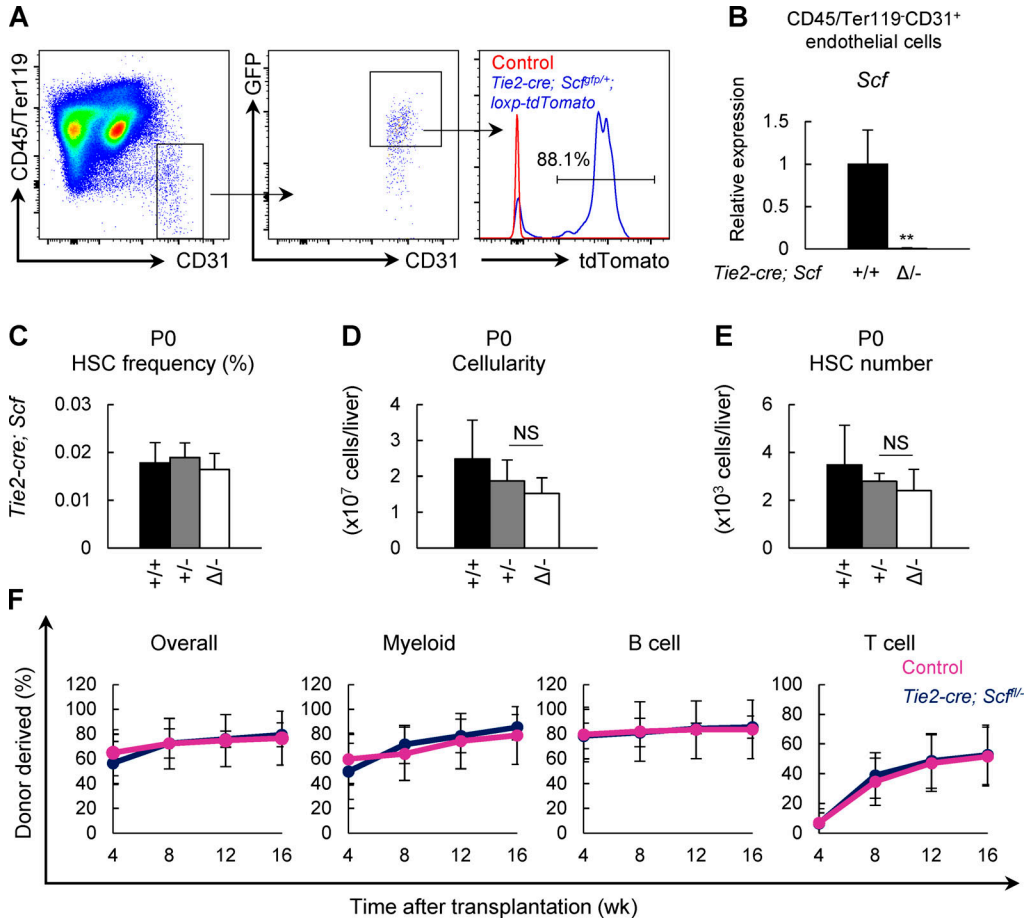

Figure 6. **Deletion of *Scf* from endothelial cells does not lead to significant reduction in HSC frequency or function in the developing liver. (A)** *Tie2-cre* recombined in the majority of CD45$^-$Ter119$^-$CD31$^+$*Scf*-GFP$^+$ endothelial cells in the *Tie2-cre; Scf$^{gfp/+}$; loxp-tdTomato* P0 livers (n = 5 mice for control, and n = 3 mice for *Tie2-cre; Scf$^{gfp/+}$; loxp-tdTomato*). **(B)** qRT-PCR analysis of *Scf* transcript levels in CD45$^-$Ter119$^-$CD31$^+$ endothelial cells sorted from P0 livers of control or *Tie2-cre; Scf$^{fl/-}$* mice (n = 3 mice for control, and n = 4 mice for *Tie2-cre; Scf$^{fl/-}$*). **(C–E)** HSC frequency (C), liver cellularity (D), and HSC number (E) in P0 *Tie2-cre; Scf$^{fl/-}$* mice compared with littermate controls (n = 7 mice for *Scf$^{+/+}$*, n = 3 mice for *Scf$^{+/-}$*, and n = 9 mice for *Tie2-cre; Scf$^{fl/-}$*). **(F)** 5 × 10^5 liver cells from *Tie2-cre; Scf$^{fl/-}$* mice gave normal levels of reconstitution in irradiated mice (data represent three independent experiments with a total of n = 15 recipients for controls and n = 16 recipients for mutants). *Scf$^{+/+}$* and *Scf$^{+/-}$* mice were used as controls. +, WT allele; Δ, recombined *Scf^{fl}* allele; –, germline deleted allele. *Scf$^{+/+}$* mice include *Cre; Scf$^{+/+}$*, *Cre; Scf$^{fl/+}$*, and *Cre*(–); *Scf$^{+/+}$* mice. *Scf$^{+/-}$* mice include *Cre; Scf$^{+/-}$* and *Cre*(–); *Scf$^{fl/-}$* mice. All data represent mean ± SD. Two-tailed Student's *t* tests were used to evaluate statistical significance. **, P < 0.01.

with hepatic stellate cells to promote HSC maintenance in the developing liver by producing SCF.

Hepatic stellate cells progressively lose HSC niche gene expression signature in the neonatal liver

From E15.5 to P5, stellate cells significantly down-regulated *Scf*-GFP expression (10.8-fold), while endothelial cells did so to a much lesser extent (2.7-fold; Fig. 9 A). These data suggest that gene expression changes in stellate cells may deplete HSC-supporting activity and drive HSC egress from the liver around birth. To study these gene expression changes in detail, we conducted a genome-wide expression profiling of hepatic stellate cells from E15.5, P5, and P10, when HSCs gradually migrate out of the liver (Fig. 1 C and Fig. S1 A). 2,441 genes were significantly up-regulated and 2,253 genes were significantly down-regulated (P ≤ 0.05, fold-change two or greater) in hepatic stellate cells comparing E15.5 to either P5 or P10 (Fig. 9 B). Gene ontology analysis using the Database for Annotation, Visualization and Integrated Discovery comparing stellate cells at E15.5 and P10 revealed several significantly enriched biological processes, including oxidation reduction, metabolic process, and liver development (Fig. 9 C).

Consistent with the loss of HSC-supporting activity from the liver by P10, gene set enrichment analysis (GSEA) showed that P10 hepatic stellate cells have expression profiles significantly depleted of hematopoietic stem and progenitor cell–supporting genes (Charbord et al., 2014) compared with those from E15.5 livers (Fig. 9 D). The expression levels of HSC-supporting factors, such as *Scf* (Barker, 1994), *Vcam1* (Dutta et al., 2015), *Pleiotrophin* (Himburg et al., 2012), and *Jagged1* (Poulos et al., 2013), in hepatic stellate cells decreased significantly over time from E15.5 to P10 (Fig. 9 E), correlating with the gradual depletion of HSC-supporting activity in the livers from E15.5 to P10. Interestingly, principal component analysis (PCA) showed that E15.5 hepatic stellate cells are more similar to bone marrow *Scf*-GFP$^+$ mesenchymal stromal cells, the key niche cells in the adult bone

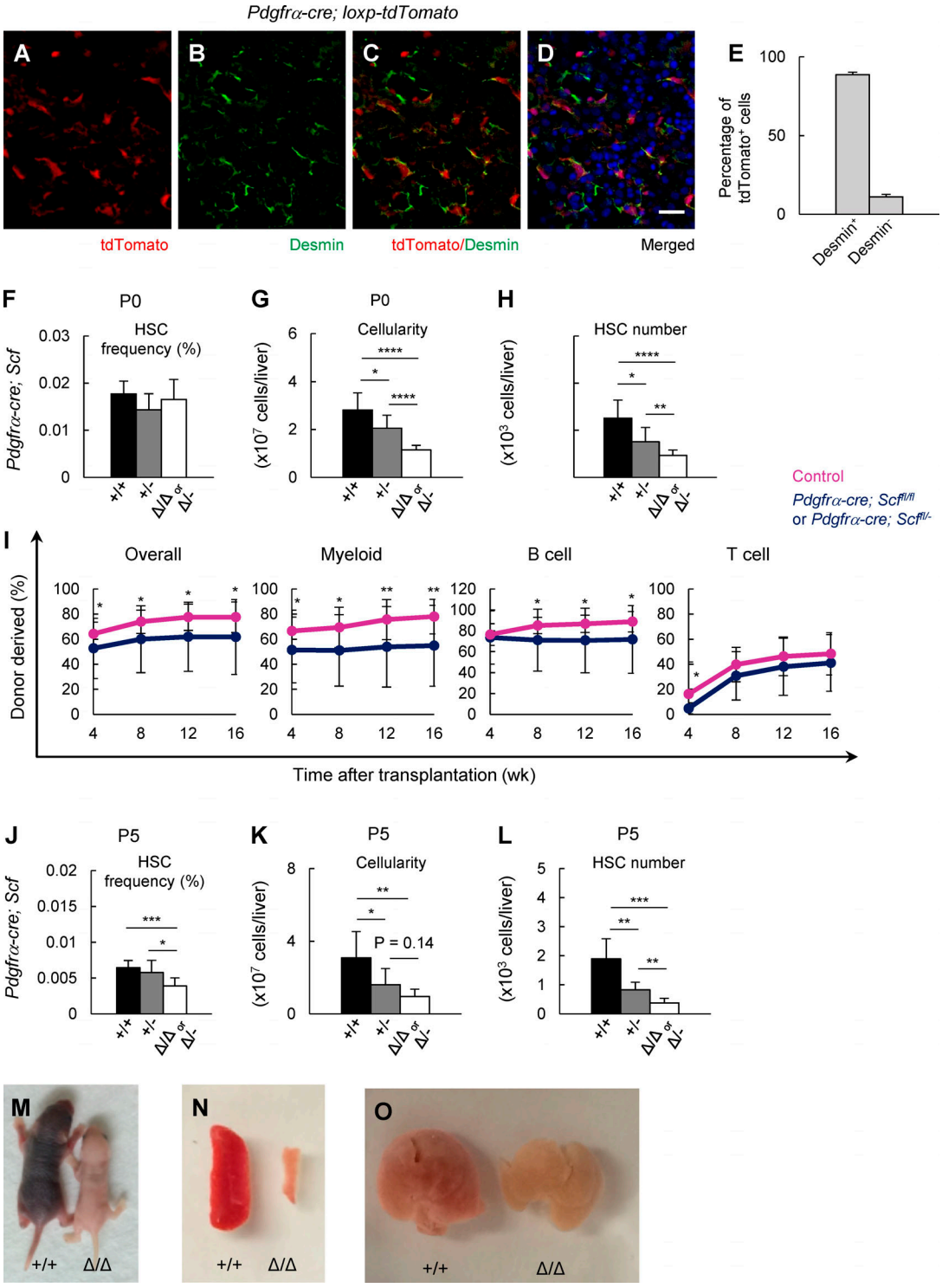

Figure 7. ***Scf* from hepatic stellate cells is required for HSC maintenance in the developing liver. (A–D)** Confocal images showing that *Pdgfrα-cre* recombined in hepatic stellate cells in the developing liver of *Pdgfrα-cre; loxp-tdTomato* mice. Hepatic stellate cells were stained with an anti-Desmin antibody. Nuclei were stained with DAPI, in blue. **(E)** Quantification of hepatic stellate cell specificity of *Pdgfrα-cre* in *Pdgfrα-cre; loxp-tdTomato* P0 livers. Cells were quantified from three independent confocal images. **(F–H)** HSC frequency (F), liver cellularity (G), and HSC number (H) in P0 livers of *Pdgfrα-cre; Scf*$^{fl/fl}$ or *Pdgfrα-cre; Scf*$^{fl/-}$ mice versus littermate controls (n = 8 mice for *Scf*$^{+/+}$, n = 6 mice for *Scf*$^{+/-}$, and n = 12 mice for *Pdgfrα-cre; Scf*$^{fl/fl}$ or *Pdgfrα-cre; Scf*$^{fl/-}$). **(I)** 5 × 10^5 liver cells from P0 *Pdgfrα-cre; Scf*$^{fl/fl}$ or *Pdgfrα-cre; Scf*$^{fl/-}$ mice gave significantly lower levels of reconstitution in irradiated mice relative to controls (data represent five independent experiments with a total of n = 23 recipients for controls and n = 22 recipients for mutants). *Scf*$^{+/+}$ and *Scf*$^{+/-}$ mice were used as controls. **(J–L)** HSC frequency (J), liver cellularity (K), and HSC number (L) in P5 livers of *Pdgfrα-cre; Scf*$^{fl/fl}$ or *Pdgfrα-cre; Scf*$^{fl/-}$ mice compared with littermate controls (n = 10 mice for *Scf*$^{+/+}$, n = 6 mice for *Scf*$^{+/-}$, and n = 6 mice for *Pdgfrα-cre; Scf*$^{fl/fl}$ or *Pdgfrα-cre; Scf*$^{fl/-}$). **(M)** Representative images of P5 *Pdgfrα-cre; Scf*$^{fl/fl}$ mice and littermate controls. **(N and O)** Representative images of spleens (N) and livers (O) of P5 *Pdgfrα-cre; Scf*$^{fl/fl}$ mice and littermate controls. +, WT allele; Δ, recombined *Scf*^{fl} allele; –, germline deleted allele. *Scf*$^{+/+}$ mice include *Cre; Scf*$^{+/+}$, *Cre; Scf*$^{fl/+}$, and *Cre*(–); *Scf*$^{+/+}$ mice. *Scf*$^{+/-}$ mice include *Cre; Scf*$^{+/-}$ and

Cre(−); $Scf^{fl/-}$ mice. All data represent mean ± SD. Two-tailed Student's *t* tests were used to evaluate statistical significance. *, P < 0.05; **, P < 0.01; ***, P < 0.001; ****, P < 0.0001. Scale bar is 20 µm in D.

marrow (Ding and Morrison, 2013; Ding et al., 2012; Lee et al., 2017), than adult hepatic stellate cells at the transcriptome level (Fig. 9 F). Collectively, these data suggest that fetal stellate cells are endowed with HSC-supporting activity, similar to adult bone marrow mesenchymal cells, and this activity is lost around birth.

Discussion

Here, we undertook a systematic genetic approach to functionally dissect the HSC niche in the developing liver in vivo. We found that HSCs localized in a perisinusoidal vascular niche where endothelial cells and hepatic stellate cells are two major cellular sources of SCF. Both cell types are functionally important as combined deletion of *Scf* from endothelial cells and hepatic stellate cells led to profound HSC depletion (Fig. 8). Hepatic stellate cells play important roles in storage of vitamin A in adult livers (Yin et al., 2013). But their role during hematopoietic development was previously unknown. Our results suggest that fetal hepatic stellate cells are a critical component of the HSC niche. Whole body deletion of stellate cell–specific transcriptional factors, *Lhx2* and *Hlx*, resulted in fetal liver hematopoietic defects in a non–cell-autonomous manner (Hentsch et al., 1996; Porter et al., 1997), supporting the notion that stellate cells are a critical component of the liver hematopoietic niche, although HSCs were not analyzed in these studies. In line with these data, fetal hepatic stellate cells are associated with hematopoietic foci and have a greater capacity in maintaining hematopoiesis in vitro than other stromal cells in the fetal liver (Kordes et al., 2013).

Our genetic approach does not distinguish the function of membrane-bound or soluble SCF, although it likely acts locally (Wolf, 1978). Consistent with this, we found that most HSCs are close to endothelial and stellate cells, the major source of SCF, in the developing liver. Through systematic conditional deletion in candidate cell types, we found that endothelial and stellate cells are the major, if not exclusive, source of SCF, as ∼90% HSCs are lost when *Scf* is deleted from both endothelial and hepatic stellate cells (Fig. 8). It is not clear why endothelial and stellate cells synergistically promote HSC maintenance. The redundancy between these cells as sources of SCF may offer extra robustness to the system, and thus an evolutional advantage. Khan et al. (2016) identified $Nestin^+NG2^+$ periportal stromal cells as an important cellular component of the fetal liver niche. However, ablation of these cells resulted in enhanced reconstitution activity, mainly in the T and B cell lineages (Khan et al., 2016), suggesting that $NG2^+$ periportal stromal cells are not required for the maintenance of functional HSCs in the fetal liver. Consistent with this, we did not observe depletion of HSC number or function when *Scf* was deleted from *Ng2-cre*–expressing cells (Fig. 5, F–I). Hepatocytes are a critical source of thrombopoietin for bone marrow HSC maintenance (Decker et al., 2018). But it appears that thrombopoietin is not required for E14.5 fetal liver HSC maintenance, suggesting distinct fetal and adult HSC maintenance mechanisms (Qian et al., 2007). Additional cell types may also contribute to the HSC niche in the developing liver by generating other HSC-supporting factors.

Murine fetal liver hematopoiesis starts from around E12.5 (Mikkola and Orkin, 2006). Blockade of the SCF-cKIT pathway by administration of cKIT functional blocking antibody after E12.5 quickly eliminates hematopoietic progenitors (within 2 d), while applying the same blocking antibody before E12.5 does not affect those progenitors, suggesting that hematopoiesis before the fetal liver stage is SCF independent (Ogawa et al., 1993). Alternatively, using a whole-body knockout approach, a recent report suggests that SCF is required for preHSCs before the fetal liver stage (Azzoni et al., 2018). Although further investigation is clearly needed to address the role of SCF in early hematopoiesis, it is well established that SCF is required for fetal liver HSCs (Broudy, 1997; Ding et al., 2012; Ikuta and Weissman, 1992). We found that conditional deletion of *Scf* from *Pdgfrα-cre* and/or *Tie2-cre*–expressing cells does not lead to HSC depletion in early (E14.5 or E15.5) livers (Fig. S5). In contrast, we observed significant HSC depletion in later (P0 and P5) developing livers (Fig. 7 and Fig. 8). Although antibody blockade has faster kinetics (Ogawa et al., 1993) than our conditional genetic models, our data suggest that the observed HSC depletion in later developmental stages in our study reflects disruption of niche function and a critical role of SCF for HSCs in the developing liver.

Materials and methods

Mice

Scf^{gfp}, Scf^{fl}, Scf^{-}, and $Cxcl12^{DsRed}$ mice were described previously (Ding and Morrison, 2013; Ding et al., 2012). *Vav1-cre* (de Boer et al., 2003), *Albumin-cre* (Weisend et al., 2009), *Tie2-cre* (Kisanuki et al., 2001), *Pdgfrα-cre* (Roesch et al., 2008), *Ng2-cre* (Zhu et al., 2008), and *loxp-tdTomato* (Madisen et al., 2010) mice were obtained from The Jackson Laboratory and maintained on C57BL/6 background. All mice were housed in a specific pathogen–free, Association for the Assessment and Accreditation of Laboratory Animal Care–approved unit at Columbia University Medical Center. All protocols were approved by Columbia University Committee on the Institute Animal Care and Use. Unless otherwise noted, data are mean ± SD, and two-tailed Student's *t* tests were used to evaluate statistical significance (*, P < 0.05; **, P < 0.01; ***, P < 0.001; ****, P < 0.0001).

Long-term competitive reconstitution assay

A cesium-137 irradiator (JL Shepherd and Associates) was used to lethally irradiate (total 1,080 rads in a split dose) adult recipient mice. After anesthetization, 5×10^5 developing liver cells along with 5×10^5 recipient bone marrow cells were retro-orbitally injected into the recipients. Mice were maintained on antibiotic water (Baytril 0.17 gl^{-1}) for 14 d after transplantation, then changed to regular water. Recipient mice were bled every 4

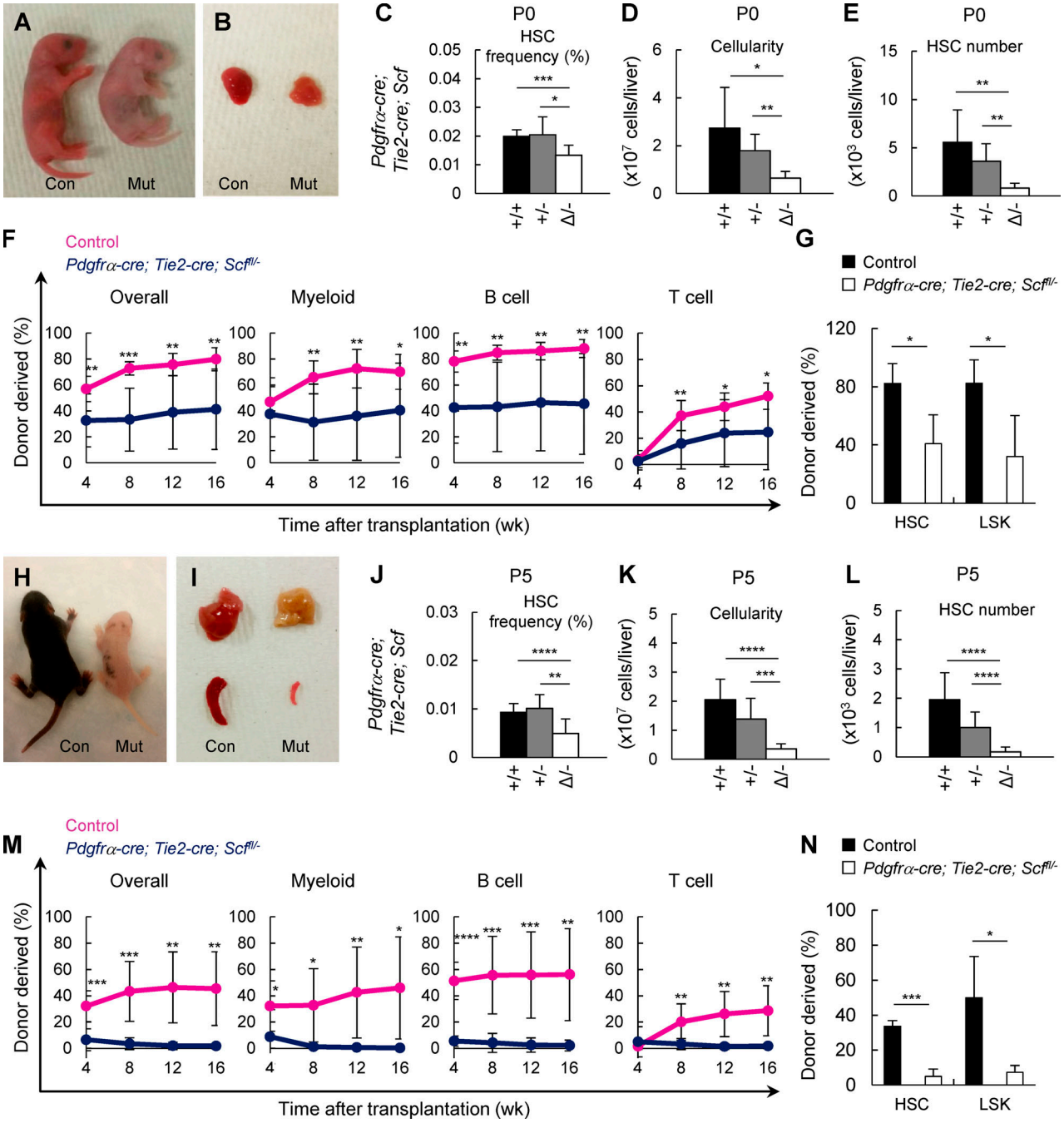

Figure 8. ***Scf* from endothelial cells and hepatic stellate cells is synergistically required for HSC maintenance in the developing liver. (A)** Representative images of P0 *Pdgfrα-cre; Tie2-cre; Scf*$^{fl/-}$ mice and littermate controls. **(B)** Representative images of livers from P0 *Pdgfrα-cre; Tie2-cre; Scf*$^{fl/-}$ mice and littermate controls. **(C–E)** HSC frequency (C), cellularity (D), and absolute HSC number (E) in P0 livers of *Pdgfrα-cre; Tie2-cre; Scf*$^{fl/-}$ mice compared with littermate controls (n = 11 mice for *Scf*$^{+/+}$, n = 4 mice for *Scf*$^{+/-}$, and n = 7 mice for *Pdgfrα-cre; Tie2-cre; Scf*$^{fl/-}$). **(F)** 5 × 10^5 liver cells from P0 *Pdgfrα-cre; Tie2-cre; Scf*$^{fl/-}$ mice gave significantly lower levels of donor reconstitution in all major hematopoietic lineages in irradiated recipient mice relative to controls (data represent three independent experiments with a total of n = 9 recipients for controls and n = 13 recipients for mutants). *Scf*$^{+/+}$ and *Scf*$^{+/-}$ mice were used as controls. **(G)** Donor-derived HSC and LSK chimerism in recipient mice 16 wk after transplantation (n = 3 mice for control, and n = 4 mice for *Pdgfrα-cre; Tie2-cre; Scf*$^{fl/-}$). **(H)** Representative images of P5 *Pdgfrα-cre; Tie2-cre; Scf*$^{fl/-}$ mice and littermate controls. **(I)** Representative images of livers and spleens of P5 *Pdgfrα-cre; Tie2-cre; Scf*$^{fl/-}$ mice and littermate controls. **(J–L)** HSC frequency (J), cellularity (K), and absolute HSC number (L) in P5 livers from *Pdgfrα-cre; Tie2-cre; Scf*$^{fl/-}$ mice compared with littermate controls (n = 16 mice for *Scf*$^{+/+}$, n = 6 mice for *Scf*$^{+/-}$, and n = 12 mice for *Pdgfrα-cre; Tie2-cre; Scf*$^{fl/-}$). **(M)** 5 × 10^5 liver cells from P5 *Pdgfrα-cre; Tie2-cre; Scf*$^{fl/-}$ mice gave significantly lower levels of donor reconstitution in all major hematopoietic lineages in irradiated recipient mice relative to controls (data represent two independent experiments with a total of n = 9 recipients and n = 7 recipients from three independent pairs of mutant and control mice). *Scf*$^{+/+}$ and *Scf*$^{+/-}$ mice were used as controls. **(N)** Donor-derived HSC and LSK chimerism in recipient mice 16 wk after transplantation (n = 3 mice for control, and n = 4 mice for *Pdgfrα-cre; Tie2-cre; Scf*$^{fl/-}$). *Scf*$^{+/+}$ includes *Pdgfrα-cre; Tie2-cre; Scf*$^{+/+}$, *Pdgfrα-cre; Scf*$^{+/+}$, *Tie2-cre; Scf*$^{+/+}$, *Pdgfrα-cre; Scf*$^{fl/+}$, *Tie2-cre; Scf*$^{fl/+}$, and *Cre(–); Scf*$^{fl/+}$ mice. *Scf*$^{+/-}$ mice include *Pdgfrα-cre; Tie2-cre; Scf*$^{+/-}$, *Pdgfrα-cre; Scf*$^{+/-}$, *Tie2-cre; Scf*$^{+/-}$, and *Cre(–); Scf*$^{+/-}$ mice. Littermate controls include *Scf*$^{+/+}$ and *Scf*$^{+/-}$ mice. All data represent mean ± SD. Two-tailed Student's t tests were used to evaluate statistical significance. *, P < 0.05; **, P < 0.01; ***, P < 0.001; ****, P < 0.0001. +, WT allele; Δ, recombined Scf^{fl} allele; –, germline deleted allele; Con, control; Mut, mutant.

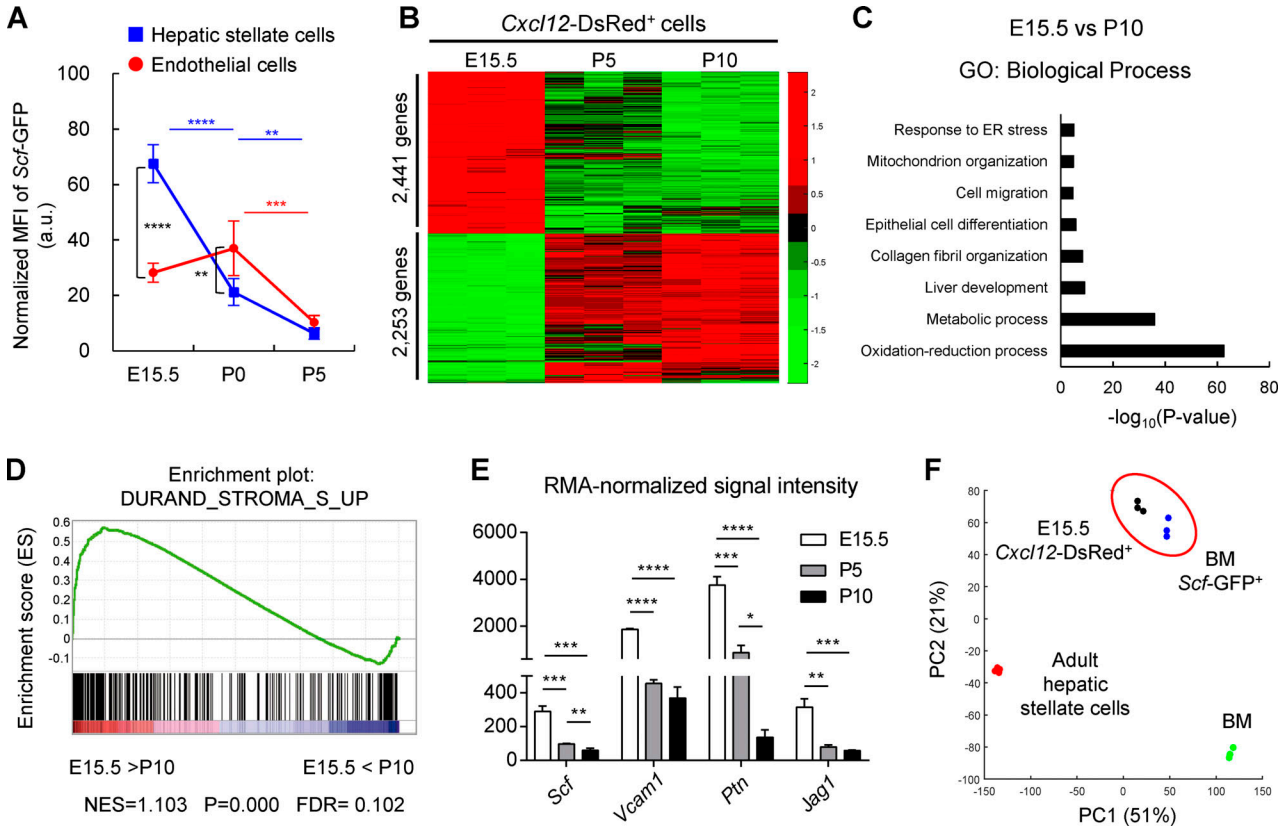

Figure 9. **Hepatic stellate cells down-regulate HSC-supporting genes in neonatal mice. (A)** Hepatic stellate cells significantly down-regulated *Scf*-GFP in the developing liver between E15.5 and P5. Endothelial cells did so to a much lesser extent. The fluorescence intensity of GFP in CD45$^+$ and/or Ter119$^+$ hematopoietic cells in each samples was used for normalization of the expression (n = 3 for E15.5 hepatic stellate cells, n = 5 for P0 hepatic stellate cells, n = 3 for P5 hepatic stellate cells, n = 6 for E15.5 endothelial cells, n = 8 for P0 endothelial cells, and n = 5 for P5 endothelial cells). **(B)** Heatmap of 4,694 differentially expressed genes between *Cxcl12*-DsRed$^+$ stellate cells from E15.5, P5, and P10 livers. 2,441 genes were significantly up-regulated and 2,253 genes were significantly down-regulated in E15.5 *Cxcl12*-DsRed$^+$ stellate cells compared with those purified from either P5 or P10 livers (n = 3 mice for each group). **(C)** Gene ontology analysis revealed biological processes significantly affected in E15.5 *Cxcl12*-DsRed$^+$ stromal cells compared with those from P10 liver. **(D)** GSEA showed significant enrichment of hematopoietic stem and progenitor cell–supporting genes down-regulated in P10 *Cxcl12*-DsRed$^+$ stellate cells compared with E15.5 *Cxcl12*-DsRed$^+$ stellate cells. **(E)** Robust multi-array average–normalized signal intensity of *Scf*, *Vcam1*, *Pleiotrophin*, and *Jagged1* in *Cxcl12*-DsRed$^+$ stellate cells at E15.5, P5, and P10. **(F)** PCA of the gene expression profiles of *Cxcl12*-DsRed$^+$ stellate cells from E15.5 livers, *Scf*-GFP$^+$ mesenchymal stromal cells from the adult bone marrow, adult hepatic stellate cells, and whole bone marrow cells. Gene expression profiles for *Scf*-GFP$^+$ mesenchymal stromal cells and adult hepatic stellate cells were from Gene Expression Omnibus datasets GSE33158 and GSE38648, respectively (n = 3 for E15.5 *Cxcl12*-DsRed$^+$, n = 3 for bone marrow [BM] *Scf*-GFP$^+$, n = 3 for BM, and n = 4 for adult hepatic stellate cells). All data represent mean ± SD. Two-tailed Student's t tests were used to evaluate statistical significance. *, P < 0.05; **, P < 0.01; ***, P < 0.001; ****, P < 0.0001. a.u., arbitrary units; BM, bone marrow; FDR, false discovery rate; GO, gene ontology; MFI, mean fluorescence intensity; NES, normalized enrichment score; RMA, robust multi-array average.

wk up to at least 16 wk after transplantation to evaluate the level of donor-derived hematopoietic lineages including myeloid, B, and T cells. Blood was incubated with ammonium chloride potassium red cell lysis before proceeding to antibody staining. Cells were stained with anti-CD45.2 (104), anti-CD45.1 (A20), anti-Gr1 (8C5), anti-Mac-1 (M1/70), anti-B220 (6B2), and anti-CD3 (KT31.1; Biolegend) and analyzed by flow cytometry. For transplantation of neonatal mice, 1 million freshly prepared bone marrow cells from CD45.1 mice were injected into the liver or temporal vein of neonatal mice (P0–P3). The mice were then followed for up to 4 mo.

Flow cytometry

Liver cells were isolated by crushing the tissue between two glass slides. The cells were passed through 25-G syringes with Ca^{2+} and Mg^{2+} free HBSS with 2% heat-inactivated bovine serum for single cell suspension. Then cells were filtered through 70-µm nylon mesh. For staining HSCs, the following antibodies were used: lineage markers (anti-Ter119, anti-B220 [6B2], anti-Gr1 [8C5], anti-CD2 [RM2-5], anti-CD3 [17A2], anti-CD5 [53–7.3], and anti-CD8 [53–6.7]), anti-CD150 (TC15-12F12.2), anti-CD48 (HM48-1), anti-Sca-1 (E13-161.7), and anti-cKit (2B8; Biolegend). DAPI was used to preclude dead cells. For flow-cytometric analysis of *Scf*-GFP$^+$, *Cxcl12*-DsRed$^+$, and endothelial cells, the tissue was digested with Collagenase IV (200 U ml^{-1}) and DNase I (200 U ml^{-1}) at 37°C for 20 min. Digested tissue was further dissociated by repetitive pipetting and passed through 70-µm nylon mesh. Samples were then stained with antibodies and assessed by flow cytometry. Anti-CD45 (30F-11) and anti-Ter119 antibodies (Biolegend) were used to label hematopoietic cells. For staining endothelial cells, samples were incubated with anti-CD31 (MEC13.3; Biolegend) antibody. To detect autofluorescence

of vitamin A, cells were excited with a 405-nm laser, and the emission signal was detected with a 450/50-nm bandpass filter. To exclude dead cells, 7-AAD (BD Pharmingen) was used. Samples were run on FACSAria II, BD LSR II, FACSCelesta, or FACSCanto flow cytometers. FACSDiva (BD) or FlowJo (Tree Star) software was used for data analysis.

Immunostaining of liver sections

Freshly dissected livers were fixed in 4% paraformaldehyde for 1–3 h followed by overnight incubation in 30% sucrose in PBS. The tissues were embedded in optimal cutting temperature compound and snap-frozen on dry ice. Liver sections were cut at 10 µm using a CryoJane system (Instrumedics) and air-dried overnight at room temperature. Sections were rehydrated in PBS for 5 min and blocked using either 5% goat serum or 5% donkey serum in PBS for 30 min. Primary antibodies were applied overnight at 4°C. Then slides were incubated in secondary antibodies at room temperature for 2 h with washes in between. Primary antibodies were rabbit-anti-Laminin antibody (L9393; Sigma-Aldrich), rabbit-anti-Desmin antibody (GTX103557; GeneTex), goat-anti-Desmin antibody (AF3844; R&D Systems) rabbit-anti-HNF4α antibody (ab201460; Abcam), goat-anti-VE-cadherin antibody (BAF1002; R&D Systems), goat-anti-Albumin-FITC antibody (A90-234F; Bethyl Laboratories), and mouse-anti-α-SMA-FITC antibody (F3777; Sigma-Aldrich). Secondary antibodies were anti-rabbit Alexa Fluor 488 (Thermo Fisher Scientific), anti-rabbit Alexa Fluor 555 (Thermo Fisher Scientific), anti-goat Alexa Fluor 488 (Thermo Fisher Scientific), anti-goat Alexa Fluor 555 (Thermo Fisher Scientific), Alexa Fluor 647–conjugated streptavidin (Jackson ImmunoResearch), and anti-FITC Alexa Fluor 488 (Jackson ImmunoResearch). For localizing CD150$^+$CD48$^-$lineage$^-$ candidate HSCs, slides were incubated in rat-anti-CD150 antibody (TC15-12F12.2; Biolegend) overnight at 4°C. CD150 was visualized by incubation in anti-rat Alexa Fluor 555 antibody (Thermo Fisher Scientific) for 2 h at room temperature with three washes in between. Rat IgG (Sigma-Aldrich) was then applied to the slides for 10 min and washed with PBS. FITC-conjugated anti-B220, anti-Gr-1, anti-Mac1, anti-CD5, anti-CD8a, anti-CD2, anti-CD3, anti-CD41, anti-Ter119, and anti-CD48 antibodies (Biolegend) along with rabbit-anti-Laminin antibody (Sigma-Aldrich) or rabbit-anti-Desmin antibody (GeneTex) were used for subsequent primary staining at 4°C overnight. Anti-FITC Alexa Fluor 488 (Jackson ImmunoResearch) and anti-rabbit Alexa Fluor 647 (Thermo Fisher Scientific) were used for secondary staining at room temperature for 2 h. Slides were mounted with Prolong gold antifade (Invitrogen), and images were acquired on Nikon Ti Eclipse confocal microscopes. For visualizing CD150$^+$CD48$^-$lineage$^-$ candidate HSCs with VE-cadherin$^+$ endothelial cells, after staining for CD150 as described above, the slides were stained with VE-cadherin antibody at 4°C overnight. Anti-goat Alexa Fluor 488 (Thermo Fisher Scientific) was used for secondary staining followed by blocking with goat serum for 1 h at room temperature. Slides were then washed with PBS and were incubated with biotin-conjugated anti-B220, anti-Gr-1, anti-Mac1, anti-CD5, anti-CD8a, anti-CD2, anti-CD3, anti-CD41, anti-Ter119, and anti-CD48 antibodies (Biolegend) at 4°C overnight. Alexa Fluor 647–conjugated streptavidin (Jackson ImmunoResearch) was applied for 2 h at room temperature.

Quantitative PCR (qPCR)

Enzymatically digested cells were sorted directly into Trizol. Total RNA was purified according to the manufacturer's instructions and subjected to reverse transcription using SuperScript III Reverse Transcriptase (Invitrogen). The levels of gene transcripts were quantified by quantitative real-time PCR using GoTaq qPCR Master Mix (Promega) on a CFX Connect Real-Time PCR Detection System (Bio-Rad). β-Actin was used to normalize the expression of genes. Primers used in this study were as follows: *Scf*: 5′-GTCACAGGATTCCCGCAG-3′ and 5′-AGCGCTGCCTTTCCTTATG-3′; *shortScf*: 5′-GAGGCCAGAAACTAGATCCTTT-3′ and 5′-TAAGGCTCCAAAAGCAAAGC-3′; *longScf*: 5′-GCCAGAAACTAGATCCTTTACTCCTGA-3′ and 5′-ACATAAATGGTTTTGTGACACTGACTCTG-3′; *Cxcl12*: 5′-TGCATCAGTGACGGTAAACCA-3′ and 5′-GTTGTTCTTCAGCCGTGCAA-3′; *Desmin*: 5′-CCTGGAGCGCAGAATCGAAT-3′ and 5′-TGAGTCAAGTCTGAAACCTTGGA-3′; *Lrat*: 5′-GCAGTTGGGACTGACTCCAT-3′ and 5′-CAGATTGCAGGAAGGGTCAT-3′; *Lhx2*: 5′-AGTGACCGGGCAGCGTTGTGT-3′; and 5′-GAGCGCGCATCACCATCTCTGA-3′; *Pdgfrα*: 5′-TTGACCCTGTTCCAGAGGAG-3′ and 5′-CACCAGGTCCGAGGAATCTA-3′; *β-actin*: 5′-GCTCTTTTCCAGCCTTCCTT-3′ and 5′-CTTCTGCATCCTGTCAGCAA-3′; *VE-cadherin:* 5′-TCCTCTGCATCCTCACCATCACA-3′ and 5′-GTAAGTGACCAACTGCTCGTGAAT-3′; and *Tie2*: 5′-ATGTGGAAGTCGAGAGGCGAT-3′ and 5′-CGAATAGCCATCCACTATTGTCC-3′. For quantifying deletion efficiency of *Vav1-cre*, CD45/Ter119$^+$ hematopoietic cells were sorted into tail DNA digestion buffer (Viagen Biotech) and digested. Genomic DNA was used as template for qPCR. The *Cxcl12* genomic region was used to normalize the input concentrations. The following primers were used: *Cxcl12* genomic region: 5′-GAGCCCAGAACTCTGCCACC-3′ and 5′-TCTTGCAAAGACCATCCCCTC-3′; and *Scf* genomic region: 5′-GGAAAAGAACCAAGTGAAGTC-3′ and 5′-GTCCGCAGCAAGCTCACCAGC-3′. *Scf*$^{fl/fl}$ genomic DNA was used as control.

Gene expression profiling and analysis

50,000 CD45$^-$Ter119$^-$*Cxcl12*-DsRed$^+$ stromal cells from freshly prepared livers of E15.5, P5, and P10 *Cxcl12*$^{DsRed/+}$ mice were sorted into Trizol by flow cytometry. Total RNA was isolated and amplified with the WT-Ovation Pico RNA Amplification system (Nugen) according to the manufacturer's instructions. Sense strand cDNA was generated using the WT-Ovation Exon Module (Nugen). Then cDNA was fragmented and labeled using FL-Ovation DNA Biotin Module V2 (Nugen). The labeled cDNA was hybridized to Affymetrix Mouse Gene ST 1.0 chips following the manufacturer's instructions. Expression values for all probes were normalized and determined using the robust multi-array average method with an Affymetrix Expression Console (Irizarry et al., 2003). Normalized data were analyzed using Transcriptome Analysis Console 2.0. Significantly up- or down-regulated genes ($P \leq 0.05$ and fold-change two or greater) were used to carry out gene ontology analysis using the Database for Annotation, Visualization and Integrated Discovery online tools (Huang et al., 2009). GSEA analysis was conducted as previously described (Subramanian et al., 2005).

A gene set of 297 genes up-regulated in the HSC supportive stromal cell lines compared with nonsupportive stromal lines (Charbord et al., 2014) was downloaded from Broad Institute website. Heatmap analysis and PCA were performed using MATLAB2016. The microarray data were deposited to the Gene Expression Omnibus under accession no. GSE159308.

Online supplemental material

Fig. S1 shows multilineage reconstitution of perinatal liver cells and perivascular localization of HSCs in the developing liver. Fig. S2 shows hepatic stellate cells are a major source of SCF in the developing liver, in addition to endothelial cells. Fig. S3 shows that HSCs are close to hepatic stellate cells in the developing liver, and $Scf^{+/-}$ developing liver structure and reconstitution activity are normal. Fig. S4 shows that the recombination pattern of *Pagfrα-cre* is specific to stellate cells in the developing liver. Fig. S5 shows that deletion of *Scf* from stellate cells does not lead to HSC depletion before E15.5 but leads to severe hematopoietic defects at P5. It also shows that deletion of *Scf* from both stellate and endothelial cells does not lead to HSC depletion before E14.5.

Acknowledgments

We thank R. Schwabe at Columbia University Irving Medical Center, New York, NY, for providing the adult hepatic stellate cell gene expression profile. We thank S. Ho at the Columbia Center for Translational Immunology, A. Figueroa at the Department of Microbiology and Immunology, and M. Kissner at the Columbia Stem Cell Initiative for flow cytometry, and T. Swayne and L. Munteanu at the Columbia Confocal and Specialized Microscopy core for confocal microscopy.

This work was supported by the Rita Allen Foundation, the Schaefer Scholar program, and the National Heart, Lung, and Blood Institute (R01HL132074 and R01HL153487). Y. Lee was supported by the Korea Foundation for Advanced Studies and the NYSTEM Columbia training program in stem cell research. This research was funded in part through the National Institutes of Health/National Cancer Institute Cancer Center Support Grant P30CA013696.

Author contributions: Y. Lee, J. Leslie, and L. Ding performed all of the experiments. Y. Yang provided technical help and performed some HSC localization experiments. Y. Lee and L. Ding designed the experiments, interpreted the results, and wrote the manuscript.

Disclosures: The authors declare no competing interests exist.

Submitted: 4 May 2020
Revised: 21 September 2020
Accepted: 15 October 2020

References

Andrae, J., R. Gallini, and C. Betsholtz. 2008. Role of platelet-derived growth factors in physiology and medicine. *Genes Dev.* 22:1276–1312. https://doi.org/10.1101/gad.1653708

Ara, T., K. Tokoyoda, T. Sugiyama, T. Egawa, K. Kawabata, and T. Nagasawa. 2003. Long-term hematopoietic stem cells require stromal cell-derived factor-1 for colonizing bone marrow during ontogeny. *Immunity.* 19: 257–267. https://doi.org/10.1016/S1074-7613(03)00201-2

Azzoni, E., V. Frontera, K.E. McGrath, J. Harman, J. Carrelha, C. Nerlov, J. Palis, S.E.W. Jacobsen, and M.F. de Bruijn. 2018. Kit ligand has a critical role in mouse yolk sac and aorta-gonad-mesonephros hematopoiesis. *EMBO Rep.* 19:e45477. https://doi.org/10.15252/embr.201745477

Barker, J.E. 1994. Sl/Sld hematopoietic progenitors are deficient in situ. *Exp. Hematol.* 22:174–177.

Barker, J.E. 1997. Early transplantation to a normal microenvironment prevents the development of Steel hematopoietic stem cell defects. *Exp. Hematol.* 25:542–547.

Broudy, V.C. 1997. Stem cell factor and hematopoiesis. *Blood.* 90:1345–1364. https://doi.org/10.1182/blood.V90.4.1345

Chagraoui, J., A. Lepage-Noll, A. Anjo, G. Uzan, and P. Charbord. 2003. Fetal liver stroma consists of cells in epithelial-to-mesenchymal transition. *Blood.* 101:2973–2982. https://doi.org/10.1182/blood-2002-05-1341

Charbord, P., C. Pouget, H. Binder, F. Dumont, G. Stik, P. Levy, F. Allain, C. Marchal, J. Richter, B. Uzan, et al. 2014. A systems biology approach for defining the molecular framework of the hematopoietic stem cell niche. *Cell Stem Cell.* 15:376–391. https://doi.org/10.1016/j.stem.2014.06.005

Chou, S., and H.F. Lodish. 2010. Fetal liver hepatic progenitors are supportive stromal cells for hematopoietic stem cells. *Proc. Natl. Acad. Sci. USA.* 107: 7799–7804. https://doi.org/10.1073/pnas.1003586107

de Boer, J., A. Williams, G. Skavdis, N. Harker, M. Coles, M. Tolaini, T. Norton, K. Williams, K. Roderick, A.J. Potocnik, and D. Kioussis. 2003. Transgenic mice with hematopoietic and lymphoid specific expression of Cre. *Eur. J. Immunol.* 33:314–325. https://doi.org/10.1002/immu.200310005

Decker, M., J. Leslie, Q. Liu, and L. Ding. 2018. Hepatic thrombopoietin is required for bone marrow hematopoietic stem cell maintenance. *Science.* 360:106–110. https://doi.org/10.1126/science.aap8861

Ding, L., and S.J. Morrison. 2013. Haematopoietic stem cells and early lymphoid progenitors occupy distinct bone marrow niches. *Nature.* 495: 231–235. https://doi.org/10.1038/nature11885

Ding, L., T.L. Saunders, G. Enikolopov, and S.J. Morrison. 2012. Endothelial and perivascular cells maintain haematopoietic stem cells. *Nature.* 481: 457–462. https://doi.org/10.1038/nature10783

Dutta, P., F.F. Hoyer, L.S. Grigoryeva, H.B. Sager, F. Leuschner, G. Courties, A. Borodovsky, T. Novobrantseva, V.M. Ruda, K. Fitzgerald, et al. 2015. Macrophages retain hematopoietic stem cells in the spleen via VCAM-1. *J. Exp. Med.* 212:497–512. https://doi.org/10.1084/jem.20141642

Ema, H., and H. Nakauchi. 2000. Expansion of hematopoietic stem cells in the developing liver of a mouse embryo. *Blood.* 95:2284–2288. https://doi.org/10.1182/blood.V95.7.2284

Greenbaum, A., Y.M. Hsu, R.B. Day, L.G. Schuettpelz, M.J. Christopher, J.N. Borgerding, T. Nagasawa, and D.C. Link. 2013. CXCL12 in early mesenchymal progenitors is required for haematopoietic stem-cell maintenance. *Nature.* 495:227–230. https://doi.org/10.1038/nature11926

Hackney, J.A., P. Charbord, B.P. Brunk, C.J. Stoeckert, I.R. Lemischka, and K.A. Moore. 2002. A molecular profile of a hematopoietic stem cell niche. *Proc. Natl. Acad. Sci. USA.* 99:13061–13066. https://doi.org/10.1073/pnas.192124499

Hentsch, B., I. Lyons, R. Li, L. Hartley, T.J. Lints, J.M. Adams, and R.P. Harvey. 1996. Hlx homeo box gene is essential for an inductive tissue interaction that drives expansion of embryonic liver and gut. *Genes Dev.* 10:70–79. https://doi.org/10.1101/gad.10.1.70

Himburg, H.A., J.R. Harris, T. Ito, P. Daher, J.L. Russell, M. Quarmyne, P.L. Doan, K. Helms, M. Nakamura, E. Fixsen, et al. 2012. Pleiotrophin regulates the retention and self-renewal of hematopoietic stem cells in the bone marrow vascular niche. *Cell Rep.* 2:964–975. https://doi.org/10.1016/j.celrep.2012.09.002

Huang, W., B.T. Sherman, and R.A. Lempicki. 2009. Systematic and integrative analysis of large gene lists using DAVID bioinformatics resources. *Nat. Protoc.* 4:44–57. https://doi.org/10.1038/nprot.2008.211

Ikuta, K., and I.L. Weissman. 1992. Evidence that hematopoietic stem cells express mouse c-kit but do not depend on steel factor for their generation. *Proc. Natl. Acad. Sci. USA.* 89:1502–1506. https://doi.org/10.1073/pnas.89.4.1502

Irizarry, R.A., B. Hobbs, F. Collin, Y.D. Beazer-Barclay, K.J. Antonellis, U. Scherf, and T.P. Speed. 2003. Exploration, normalization, and summaries of high density oligonucleotide array probe level data. *Biostatistics.* 4:249–264. https://doi.org/10.1093/biostatistics/4.2.249

Iwasaki, H., F. Arai, Y. Kubota, M. Dahl, and T. Suda. 2010. Endothelial protein C receptor-expressing hematopoietic stem cells reside in the perisinusoidal niche in fetal liver. *Blood.* 116:544–553. https://doi.org/10.1182/blood-2009-08-240903

Khan, J.A., A. Mendelson, Y. Kunisaki, A. Birbrair, Y. Kou, A. Arnal-Estapé, S. Pinho, P. Ciero, F. Nakahara, A. Ma'ayan, et al. 2016. Fetal liver hematopoietic stem cell niches associate with portal vessels. *Science*. 351: 176–180. https://doi.org/10.1126/science.aad0084

Kisanuki, Y.Y., R.E. Hammer, J. Miyazaki, S.C. Williams, J.A. Richardson, and M. Yanagisawa. 2001. Tie2-Cre transgenic mice: a new model for endothelial cell-lineage analysis in vivo. *Dev. Biol.* 230:230–242. https://doi.org/10.1006/dbio.2000.0106

Kordes, C., I. Sawitza, S. Götze, and D. Häussinger. 2013. Hepatic stellate cells support hematopoiesis and are liver-resident mesenchymal stem cells. *Cell. Physiol. Biochem.* 31:290–304. https://doi.org/10.1159/000343368

Kubota, H., H.L. Yao, and L.M. Reid. 2007. Identification and characterization of vitamin A-storing cells in fetal liver: implications for functional importance of hepatic stellate cells in liver development and hematopoiesis. *Stem Cells*. 25:2339–2349. https://doi.org/10.1634/stemcells.2006-0316

Lee, Y., M. Decker, H. Lee, and L. Ding. 2017. Extrinsic regulation of hematopoietic stem cells in development, homeostasis and diseases. *Wiley Interdiscip. Rev. Dev. Biol.* 6:e279. https://doi.org/10.1002/wdev.279

Li, R., K. Bernau, N. Sandbo, J. Gu, S. Preissl, and X. Sun. 2018. *Pdgfra* marks a cellular lineage with distinct contributions to myofibroblasts in lung maturation and injury response. *eLife*. 7:e36865. https://doi.org/10.7554/eLife.36865

Madisen, L., T.A. Zwingman, S.M. Sunkin, S.W. Oh, H.A. Zariwala, H. Gu, L.L. Ng, R.D. Palmiter, M.J. Hawrylycz, A.R. Jones, et al. 2010. A robust and high-throughput Cre reporting and characterization system for the whole mouse brain. *Nat. Neurosci.* 13:133–140. https://doi.org/10.1038/nn.2467

Mederacke, I., C.C. Hsu, J.S. Troeger, P. Huebener, X. Mu, D.H. Dapito, J.P. Pradere, and R.F. Schwabe. 2013. Fate tracing reveals hepatic stellate cells as dominant contributors to liver fibrosis independent of its aetiology. *Nat. Commun.* 4:2823. https://doi.org/10.1038/ncomms3823

Mikkola, H.K.A., and S.H. Orkin. 2006. The journey of developing hematopoietic stem cells. *Development*. 133:3733–3744. https://doi.org/10.1242/dev.02568

Moore, K.A., H. Ema, and I.R. Lemischka. 1997. In vitro maintenance of highly purified, transplantable hematopoietic stem cells. *Blood*. 89:4337–4347. https://doi.org/10.1182/blood.V89.12.4337

Morrison, S.J., and D.T. Scadden. 2014. The bone marrow niche for haematopoietic stem cells. *Nature*. 505:327–334. https://doi.org/10.1038/nature12984

Morrison, S.J., H.D. Hemmati, A.M. Wandycz, and I.L. Weissman. 1995. The purification and characterization of fetal liver hematopoietic stem cells. *Proc. Natl. Acad. Sci. USA*. 92:10302–10306. https://doi.org/10.1073/pnas.92.22.10302

Ogawa, M., S. Nishikawa, K. Yoshinaga, S. Hayashi, T. Kunisada, J. Nakao, T. Kina, T. Sudo, H. Kodama, and S. Nishikawa. 1993. Expression and function of c-Kit in fetal hemopoietic progenitor cells: transition from the early c-Kit-independent to the late c-Kit-dependent wave of hemopoiesis in the murine embryo. *Development*. 117:1089–1098.

Porter, F.D., J. Drago, Y. Xu, S.S. Cheema, C. Wassif, S.P. Huang, E. Lee, A. Grinberg, J.S. Massalas, D. Bodine, et al. 1997. Lhx2, a LIM homeobox gene, is required for eye, forebrain, and definitive erythrocyte development. *Development*. 124:2935–2944.

Poulos, M.G., P. Guo, N.M. Kofler, S. Pinho, M.C. Gutkin, A. Tikhonova, I. Aifantis, P.S. Frenette, J. Kitajewski, S. Rafii, and J.M. Butler. 2013. Endothelial Jagged-1 is necessary for homeostatic and regenerative hematopoiesis. *Cell Rep.* 4:1022–1034. https://doi.org/10.1016/j.celrep.2013.07.048

Qian, H., N. Buza-Vidas, C.D. Hyland, C.T. Jensen, J. Antonchuk, R. Månsson, L.A. Thoren, M. Ekblom, W.S. Alexander, and S.E. Jacobsen. 2007. Critical role of thrombopoietin in maintaining adult quiescent hematopoietic stem cells. *Cell Stem Cell*. 1:671–684. https://doi.org/10.1016/j.stem.2007.10.008

Roesch, K., A.P. Jadhav, J.M. Trimarchi, M.B. Stadler, B. Roska, B.B. Sun, and C.L. Cepko. 2008. The transcriptome of retinal Müller glial cells. *J. Comp. Neurol.* 509:225–238. https://doi.org/10.1002/cne.21730

Subramanian, A., P. Tamayo, V.K. Mootha, S. Mukherjee, B.L. Ebert, M.A. Gillette, A. Paulovich, S.L. Pomeroy, T.R. Golub, E.S. Lander, and J.P. Mesirov. 2005. Gene set enrichment analysis: a knowledge-based approach for interpreting genome-wide expression profiles. *Proc. Natl. Acad. Sci. USA*. 102:15545–15550. https://doi.org/10.1073/pnas.0506580102

Sugiyama, T., H. Kohara, M. Noda, and T. Nagasawa. 2006. Maintenance of the hematopoietic stem cell pool by CXCL12-CXCR4 chemokine signaling in bone marrow stromal cell niches. *Immunity*. 25:977–988. https://doi.org/10.1016/j.immuni.2006.10.016

Tsai, S., S.G. Emerson, C.A. Sieff, and D.G. Nathan. 1986. Isolation of a human stromal cell strain secreting hemopoietic growth factors. *J. Cell. Physiol.* 127:137–145. https://doi.org/10.1002/jcp.1041270117

Tsutsumi, M., A. Takada, and S. Takase. 1987. Characterization of desmin-positive rat liver sinusoidal cells. *Hepatology*. 7:277–284. https://doi.org/10.1002/hep.1840070212

Wandzioch, E., A. Kolterud, M. Jacobsson, S.L. Friedman, and L. Carlsson. 2004. Lhx2-/- mice develop liver fibrosis. *Proc. Natl. Acad. Sci. USA*. 101: 16549–16554. https://doi.org/10.1073/pnas.0404678101

Weisend, C.M., J.A. Kundert, E.S. Suvorova, J.R. Prigge, and E.E. Schmidt. 2009. Cre activity in fetal albCre mouse hepatocytes: Utility for developmental studies. *Genesis*. 47:789–792.

Wolf, N.S. 1978. Dissecting the hematopoietic microenvironment. III. Evidence for a positive short range stimulus for cellular proliferation. *Cell Tissue Kinet.* 11:335–345.

Wright, J.H., M.M. Johnson, M. Shimizu-Albergine, R.L. Bauer, B.J. Hayes, J. Surapisitchat, K.L. Hudkins, K.J. Riehle, S.C. Johnson, M.M. Yeh, et al. 2014. Paracrine activation of hepatic stellate cells in platelet-derived growth factor C transgenic mice: evidence for stromal induction of hepatocellular carcinoma. *Int. J. Cancer*. 134:778–788. https://doi.org/10.1002/ijc.28421

Yin, C., K.J. Evason, K. Asahina, and D.Y. Stainier. 2013. Hepatic stellate cells in liver development, regeneration, and cancer. *J. Clin. Invest.* 123: 1902–1910. https://doi.org/10.1172/JCI66369

Zhang, H., Z. Miao, Z. He, Y. Yang, Y. Wang, and M. Feng. 2005. The existence of epithelial-to-mesenchymal cells with the ability to support hematopoiesis in human fetal liver. *Cell Biol. Int.* 29:213–219. https://doi.org/10.1016/j.cellbi.2004.12.007

Zhu, X., D.E. Bergles, and A. Nishiyama. 2008. NG2 cells generate both oligodendrocytes and gray matter astrocytes. *Development*. 135:145–157. https://doi.org/10.1242/dev.004895

JEM

Supplemental material

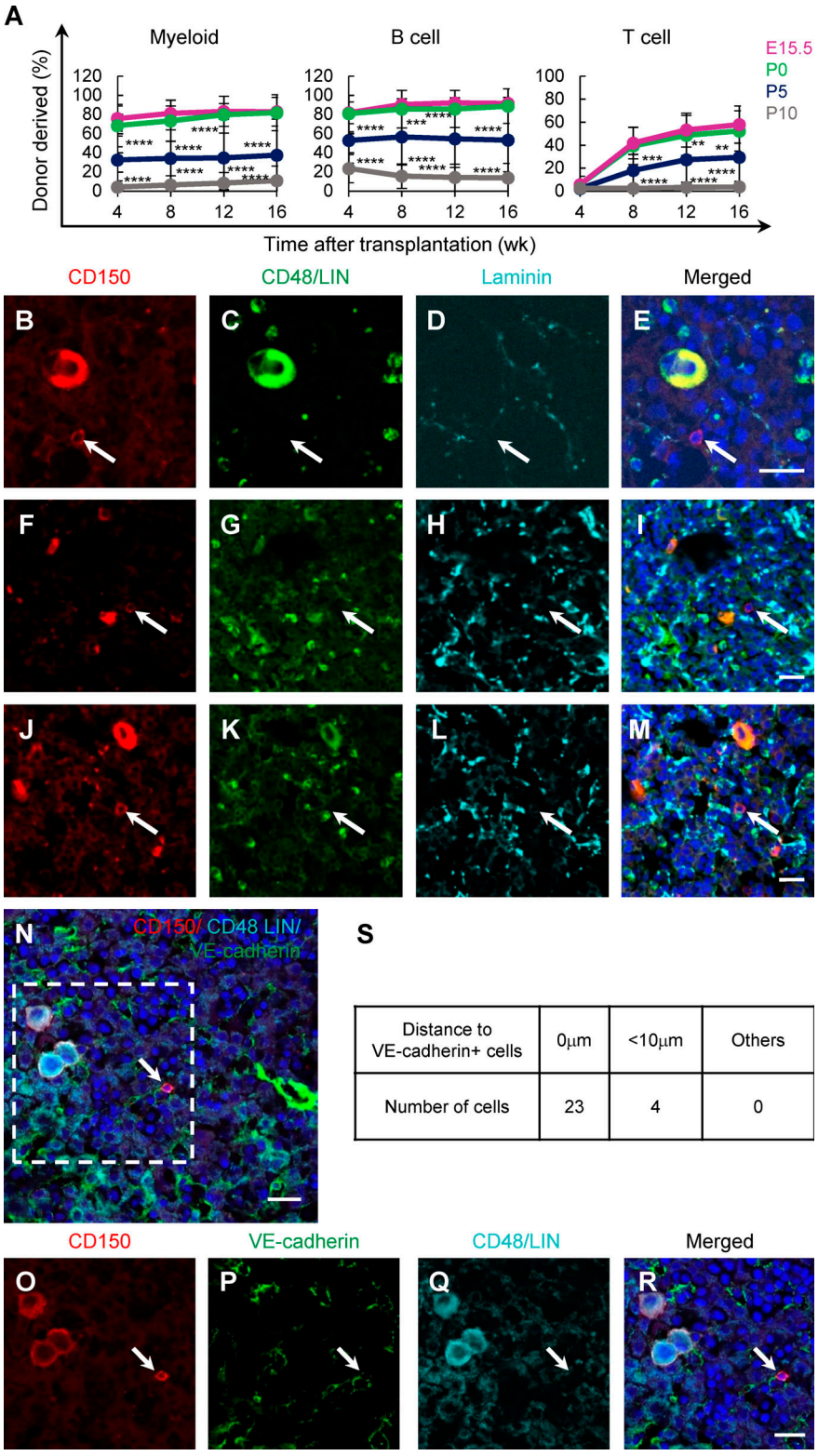

Figure S1. **HSCs are closely associated with perisinusoidal endothelial cells in the P0 liver. (A)** Long-term multilineage reconstitution assays as described in Fig. 1 C (n = 4 embryos for E15.5, n = 62 mice for P0, n = 11 mice for P5, and n = 20 mice for P10). **(B–E)** Representative images of $CD150^+CD48^-Lin^-$ candidate HSCs (arrows) localized adjacent to sinusoidal endothelial cells in the P0 liver. Endothelial cells were stained with an anti-Laminin antibody. Nuclei were stained with DAPI, in blue. **(F–M)** Representative images of $CD150^+CD48^-Lin^-$ candidate HSCs (arrows) localized adjacent to sinusoidal endothelial cells in the E15.5 liver. Endothelial cells were stained with an anti-Laminin antibody. Nuclei were stained with DAPI, in blue. **(N)** An expanded inset of the image shown in R. **(O–R)** A $CD150^+CD48^-Lin^-$ candidate HSC (arrow) is adjacent to VE-cadherin$^+$ endothelial cells. **(S)** Quantification of HSC localization relative to VE-cadherin$^+$ endothelial cells. A total of 27 HSCs were quantified from two biological replicates. Scale bars are 20 μm in E, I, M, N, and R. **, $P < 0.01$; ***, $P < 0.001$; ****, $P < 0.0001$.

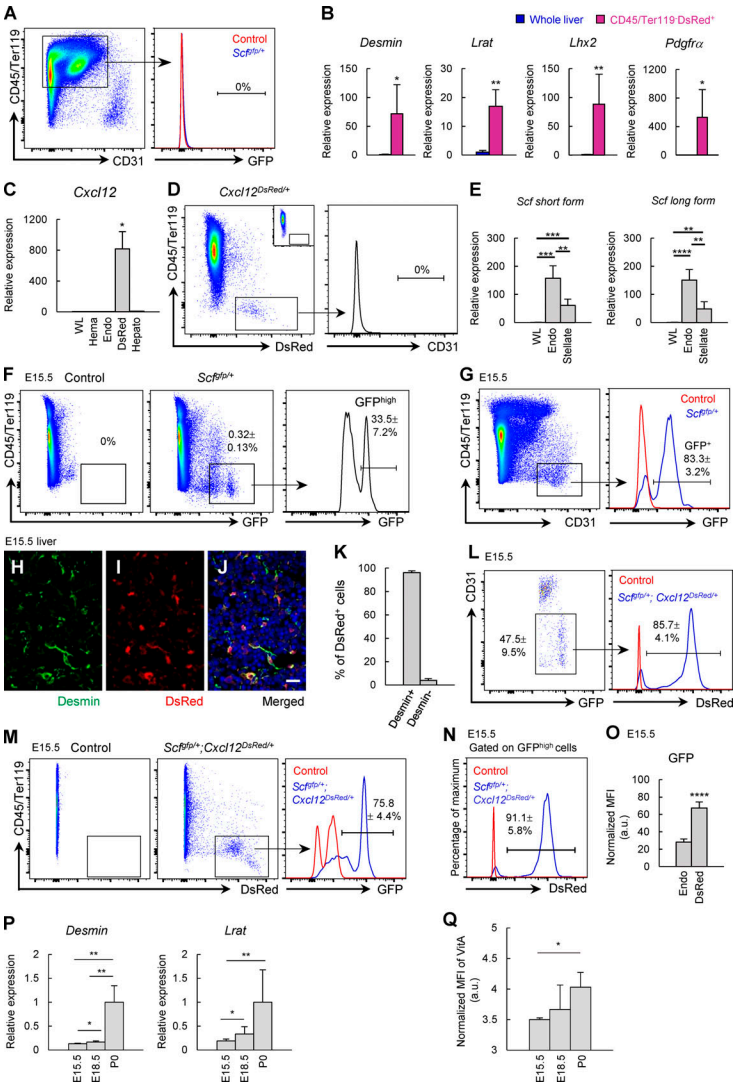

Figure S2. **Endothelial cells and hepatic stellate cells are the major sources of SCF in the developing liver. (A)** Representative flow-cytometric plots showing that CD45/Ter119$^+$ hematopoietic cells from livers of P0 *Scf*$^{gfp/+}$ mice did not express *Scf*-GFP (n = 5 mice for control, and n = 5 mice for *Scf*$^{gfp/+}$). **(B)** CD45$^-$Ter119$^-$*Cxcl12*-DsRed$^+$ stromal cells had significantly higher expression of *Desmin*, *Lrat*, *Lhx2*, and *Pdgfrα* compared with whole P0 liver cells as revealed by qRT-PCR analysis (n = 5 for whole P0 liver cells, and n = 3 for CD45$^-$Ter119$^-$*Cxcl12*-DsRed$^+$ cells). **(C)** *Cxcl12* transcript levels in different cell populations of P0 liver as quantified by qRT-PCR (n = 3 for whole liver cells [WL], n = 3 for CD45$^+$ or Ter119$^+$ hematopoietic cells [Hema], n = 3 for CD45$^-$Ter119$^-$CD31$^+$ endothelial cells [Endo], n = 4 for CD45$^-$Ter119$^-$*Cxcl12*-DsRed$^+$ stellate cells [DsRed], and n = 4 for CD45$^-$Ter119$^-$tdTomato$^+$ hepatocyte lineage cells from *Albumin-cre; loxp-tdTomato* mice [Hepato]). *Cxcl12* was highly expressed by *Cxcl12*-DsRed$^+$ hepatic stellate cells with little if any expressed by other cells in the P0 liver. **(D)** Representative flow-cytometric plots of enzymatically digested P0 *Cxcl12*$^{DsRed/+}$ livers show that CD45$^-$Ter119$^-$*Cxcl12*-DsRed$^+$ stromal cells did not express CD31, an endothelial cell marker (n = 5 mice from two independent experiments). **(E)** qRT-PCR analysis of short and long forms of *Scf* transcript levels in endothelial and stellate cells of P0 livers (n = 5 for WL, n = 3 for Endo, and n = 5 for DsRed$^+$ stellate cells). **(F)** Representative flow-cytometric plots showing that *Scf*-GFP was expressed by rare nonhematopoietic cells in E15.5 livers. Among *Scf*-GFP$^+$ stromal cells, there was a subset that expressed higher levels of *Scf*-GFP, denoted as GFP^{high} (n = 3 embryos for control, and n = 6 embryos for *Scf*$^{gfp/+}$). **(G)** Representative flow-cytometric plots showing that the majority of CD45$^-$Ter119$^-$CD31$^+$ endothelial cells in the E15.5 livers expressed *Scf*-GFP (n = 3 embryos for control, and n = 6 embryos for *Scf*$^{gfp/+}$). **(H–J)** Representative confocal images showing that virtually all *Cxcl12*-DsRed$^+$ cells expressed Desmin, a stellate cell marker, in the E15.5 liver. **(K)** Quantification of *Cxcl12*-DsRed$^+$ cells that expressed Desmin in E15.5 *Cxcl12*$^{DsRed/+}$ livers. The data are from three independent confocal images. **(L)** Representative flow-cytometric plots showing that the majority of CD45$^-$Ter119$^-$CD31$^-$*Scf*-GFP$^+$ nonendothelial stromal cells were *Cxcl12*-DsRed$^+$ stellate cells in E15.5 livers (n = 3 embryos for control, and n = 3 embryos for *Scf*$^{gfp/+}$; *Cxcl12*$^{DsRed/+}$). Note that at this stage, stellate cells expressed higher levels of *Scf* compared with endothelial cells. **(M)** The majority of CD45$^-$Ter119$^-$*Cxcl12*-DsRed$^+$ stellate cells express *Scf*-GFP in *Scf*$^{gfp/+}$; *Cxcl12*$^{DsRed/+}$ mice (n = 3 embryos for control, and n = 3 embryos for *Scf*$^{gfp/+}$; *Cxcl12*$^{DsRed/+}$). **(N)** The vast majority of CD45$^-$Ter119$^-$GFP^{high} cells, denoted as GFP^{high} cells in F, were *Cxcl12*-DsRed$^+$ stellate cells in E15.5 livers (n = 3 embryos for control, and n = 3 embryos for *Scf*$^{gfp/+}$; *Cxcl12*$^{DsRed/+}$). **(O)** CD45$^-$Ter119$^-$*Cxcl12*-DsRed$^+$ cells expressed higher levels of *Scf*-GFP compared with CD45$^-$Ter119$^-$CD31$^+$ endothelial cells in the *Scf*$^{gfp/+}$ E15.5 livers. The fluorescence intensity of GFP in CD45/Ter119$^+$ hematopoietic cells in each samples was used for normalization of the expression of *Scf*-GFP$^+$ (n = 6 for Endo, and n = 3 for DsRed$^+$ stellate cells). **(P)** qRT-PCR analyses show that CD45$^-$Ter119$^-$*Cxcl12*-DsRed$^+$ cells gradually up-regulated the expression of *Desmin* and *Lrat* during development (n = 4–7 embryos or mice per time point). **(Q)** CD45$^-$Ter119$^-$*Cxcl12*-DsRed$^+$ stellate cells gradually up-regulate the accumulation of vitamin A (VitA; n = 3–6 embryos or mice per time point). All data represent mean ± SD. Two-tailed Student's t tests were used to evaluate statistical significance. *, P < 0.05; **, P < 0.01; ***, P < 0.001; ****, P < 0.0001. Scale bar is 20 µm in J. a.u., arbitrary units; MFI, mean fluorescence intensity.

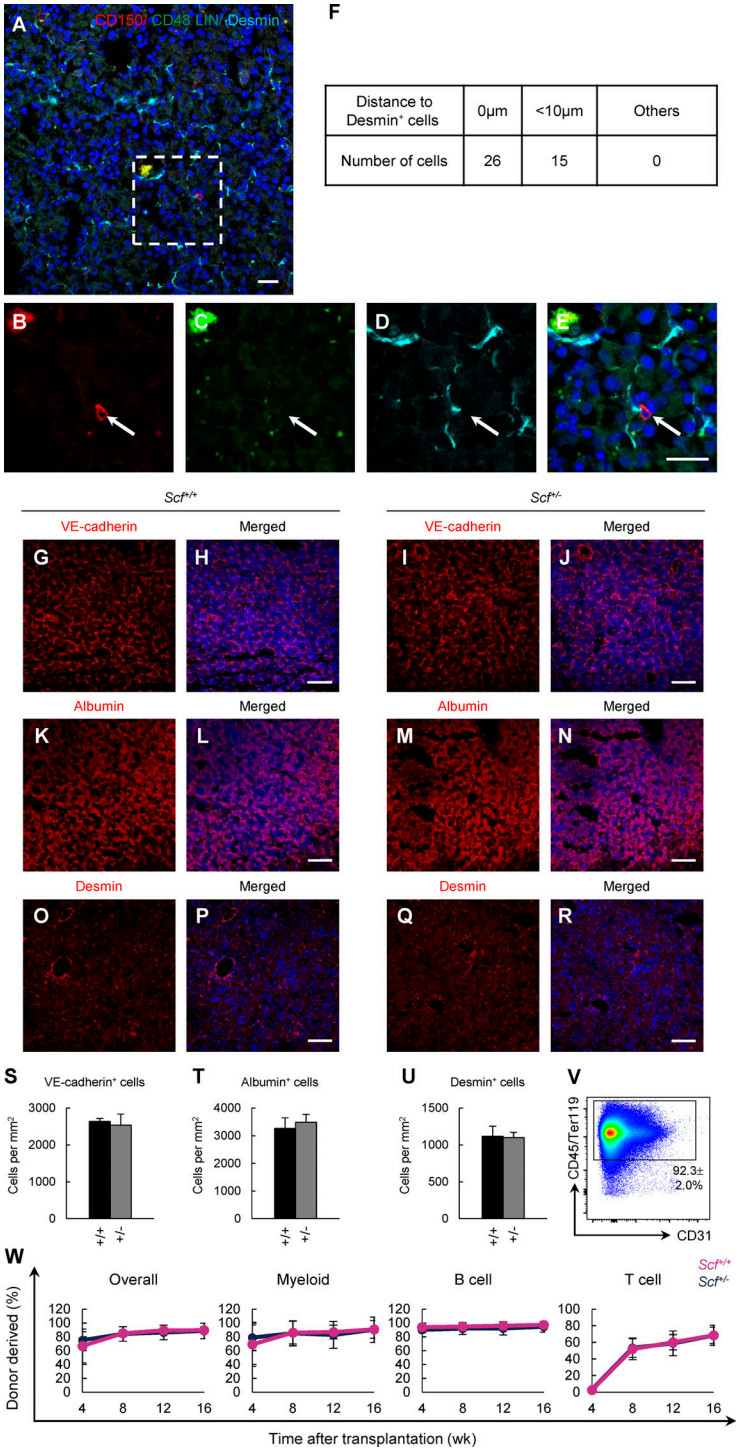

Distance to Desmin+ cells	0μm	<10μm	Others
Number of cells	26	15	0

Figure S3. **HSCs localize adjacent to Desmin⁺ hepatic stellate cells in the P0 liver, and *Scf*$^{+/-}$ P0 livers have normal number, distribution of major stromal cells, and reconstitution activity. (A)** An expanded inset of the image shown in E. **(B–E)** Representative confocal images showing that HSCs were closely associated with perisinusoidal hepatic stellate cells. HSCs were marked as CD150⁺CD48⁻Lin⁻ cells. Hepatic stellate cells were stained with an anti-Desmin antibody. Nuclei were stained with DAPI, in blue. **(F)** Quantification of distance distribution between CD150⁺CD48⁻Lin⁻ candidate HSCs and Desmin⁺ stellate cells. Measurements for all images were performed using ImageJ software. A total of 41 HSCs were quantified from two independent experiments. **(G–R)** *Scf*$^{+/-}$ P0 livers had normal numbers and distribution of VE-cadherin⁺ endothelial (G–J), Albumin⁺ hepatic (K–N), and Desmin⁺ stellate (O–R) cells compared with *Scf*$^{+/+}$ littermate controls. Nuclei were stained with DAPI, in blue. **(S–U)** Quantification of the numbers of VE-cadherin⁺ (S), Albumin⁺ (T), and Desmin⁺ (U) cells per square millimeter shown in G–R. Three representative independent regions from H, J, L, N, P, and R were used for quantification. **(V)** A representative flow-cytometric plot showing that CD45⁺ or Ter119⁺ hematopoietic cells constitute ∼92% of the total cells of enzymatically digested P0 WT livers (n = 5 from three independent experiments). **(W)** 5 × 10^5 P0 liver cells from *Scf*$^{+/-}$ mice gave similar reconstitution activity compared with littermate *Scf*$^{+/+}$ mice (n = 5 mice for *Scf*$^{+/+}$, and n = 9 mice for *Scf*$^{+/-}$). All data represent mean ± SD. Scale bars are 20 μm in A and E. Scale bars are 100 μm in H, J, L, N, P, and R.

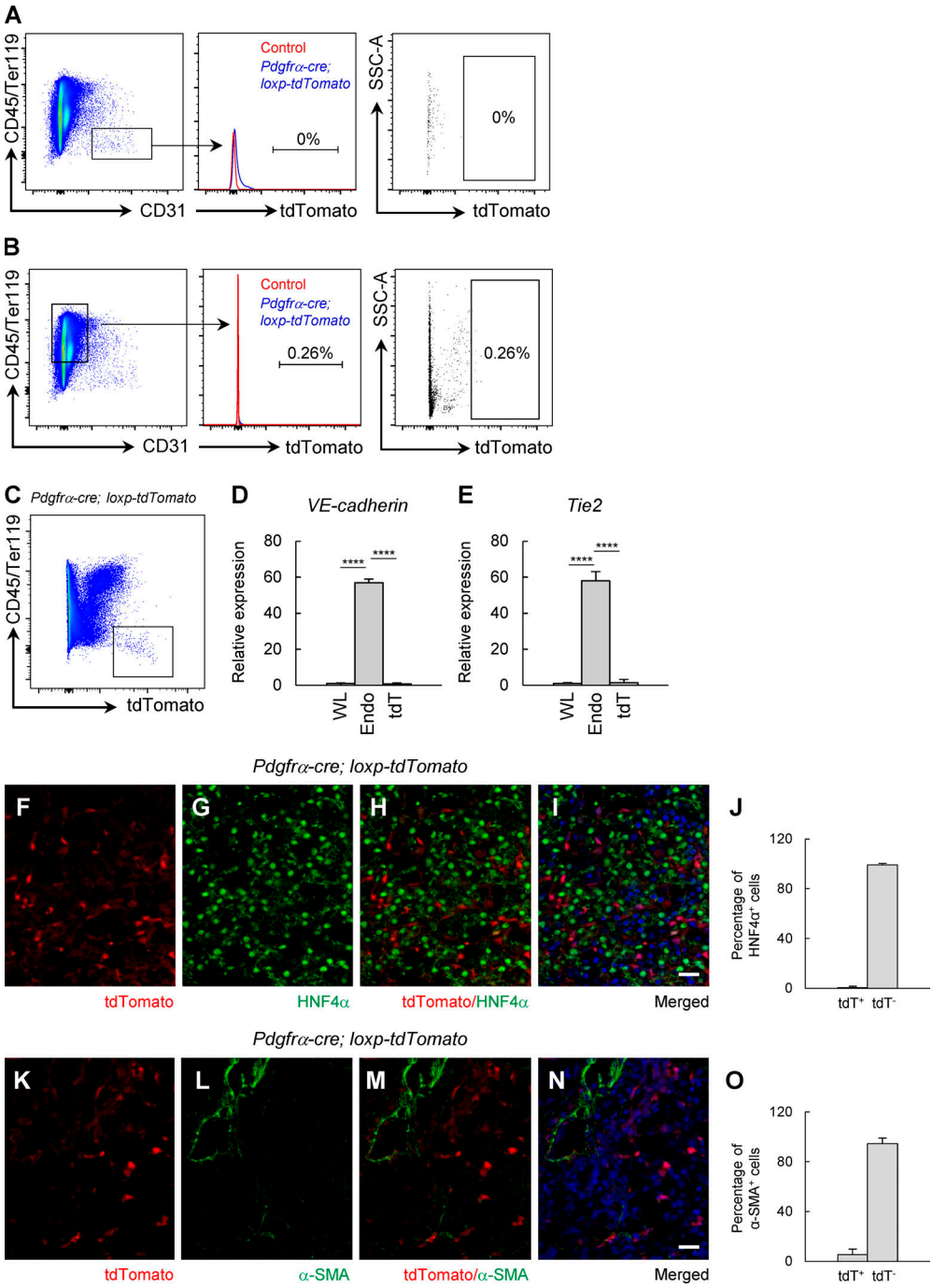

Figure S4. **Characterization of *Pdgfrα-cre* deletion pattern in the developing liver. (A)** Representative flow-cytometric plots showing that minimal if any CD45$^-$Ter119$^-$CD31$^+$ endothelial cells were labeled in the P0 livers from *Pdgfrα-cre; loxp-tdTomato* mice (n = 3 mice for control, and n = 3 mice for *Pdgfrα-cre; loxp-tdTomato*). **(B)** A representative flow-cytometric plot showing that minimal if any CD45$^+$ and/or Ter119$^+$ hematopoietic cells were labeled in the P0 livers from *Pdgfrα-cre; loxp-tdTomato* mice (n = 3 mice for control, and n = 3 mice for *Pdgfrα-cre; loxp-tdTomato*). **(C)** A representative flow-cytometric plot of gating strategy for CD45$^-$Ter119$^-$tdTomato$^+$ stromal cells purified from *Pdgfrα-cre; loxp-tdTomato* P0 livers used in D and E. **(D and E)** *VE-cadherin* (D) and *Tie2* (E) transcript levels in different cell populations of P0 livers as measured by qRT-PCR showing that *Pdgfrα-cre* recombined in minimal if any endothelial cells (n = 4 for whole liver cells [WL], n = 4 for CD45$^-$Ter119$^-$CD31$^+$ endothelial cells [Endo], and n = 3 for CD45$^-$Ter119$^-$tdTomato$^+$ stellate cells from *Pdgfrα-cre; loxp-tdTomato* P0 livers [tdT]). **(F–I)** Representative confocal images showing that *Pdgfrα-cre* does not recombine in HNF4α$^+$ hepatic lineage cells in the P0 liver. Hepatic cells were labeled with an anti-HNF4α antibody. Nuclei were stained with DAPI, in blue. **(J)** Quantification of HNF4α$^+$ hepatic lineage cells from confocal images of *Pdgfrα-cre; loxp-tdTomato* P0 liver tissue sections. Only 0.6% of hepatic lineage cells were tdTomato$^+$. The data were from three independent confocal images. **(K–N)** Representative confocal images showing that *Pdgfrα-cre* recombines in a minority of α-SMA$^+$ periportal stromal cells in the P0 liver. Periportal stromal cells were stained with an anti-α-SMA antibody. Nuclei were stained with DAPI, in blue. **(O)** Quantification of α-SMA$^+$ cells from confocal images of *Pdgfrα-cre; loxp-tdTomato* P0 liver tissue sections. Only 5% α-SMA$^+$ periportal stromal cells are tdTomato$^+$. The data were from three independent confocal images. All data represent mean ± SD. Two-tailed Student's t tests were used to evaluate statistical significance. ****, P < 0.0001. Scale bars are 20 µm in I and N. SSC-A, side scatter area.

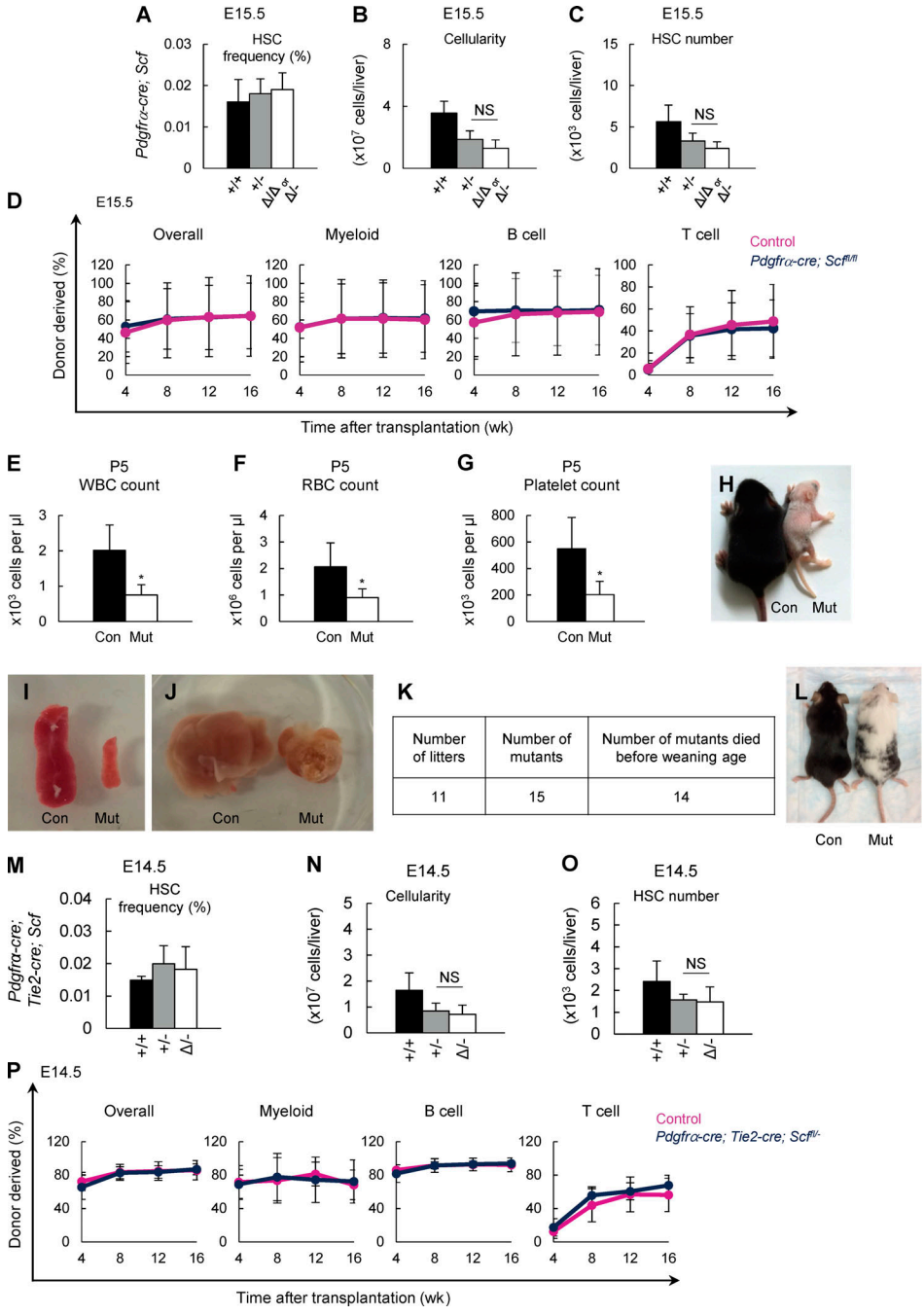

Figure S5. **Progressive loss of HSCs in the developing liver when *Scf* is deleted from stellate cells and endothelial cells. (A–C)** HSC frequency (A), cellularity (B), and HSC number (C) in livers from E15.5 *Pdgfrα-cre; Scf*$^{fl/fl}$ mice and littermate controls (n = 9 embryos for *Scf*$^{+/+}$, n = 6 embryos for *Scf*$^{+/-}$, and n = 8 embryos for *Pdgfrα-cre; Scf*$^{fl/fl}$ or *Pdgfrα-cre; Scf*$^{fl/-}$). **(D)** 5 × 10^5 liver cells from E15.5 *Pdgfrα-cre; Scf*$^{fl/fl}$ mice gave normal levels of reconstitution in irradiated mice (data represent a total of n = 7 recipients for controls and n = 10 recipients for mutants from two independent experiments). *Pdgfrα-cre; Scf*$^{+/+}$ and *Pdgfrα-cre; Scf*$^{fl/+}$ mice were used as controls. **(E–G)** P5 *Pdgfrα-cre; Scf*$^{fl/fl}$ mice had significant reduction in white blood cell (WBC) count (E), RBC count (F), and platelet count (G; n = 6 mice for controls [Con], and n = 4 mice for mutants [Mut]). **(H)** A representative image of P10 *Pdgfrα-cre; Scf*$^{fl/fl}$ mice and littermate controls. **(I and J)** Representative images of spleens (I) and livers (J) from P10 *Pdgfrα-cre; Scf*$^{fl/fl}$ mice and littermate controls. **(K)** 14 out of 15 *Pdgfrα-cre; Scf*$^{fl/fl}$ pups died early postnatally, mostly before weaning age, while none of the controls (n = 63) did so. The one surviving *Pdgfrα-cre; Scf*$^{fl/fl}$ mouse was smaller and paler compared with littermate controls. **(L)** A representative image of *Pdgfrα-cre; Scf*$^{fl/fl}$ and control mice at 4 mo after being intravenously transplanted with 1 million bone marrow cells at P0–P3. **(M–O)** HSC frequency (M), cellularity (N), and absolute HSC number (O) in E14.5 livers from *Pdgfra-cre; Tie2-cre; Scf*$^{fl/-}$ mice compared with littermate controls (n = 3 embryos for *Scf*$^{+/+}$, n = 4 embryos for *Scf*$^{+/-}$, and n = 3 embryos for *Pdgfra-cre; Tie2-cre; Scf*$^{fl/-}$). **(P)** 5 × 10^5 liver cells from E14.5 *Pdgfra-cre; Tie2-cre; Scf*$^{fl/-}$ mice gave normal donor reconstitution in all major hematopoietic lineages in irradiated recipient mice (data represent two independent experiments with a total of n = 8 recipients for controls and n = 6 recipients for mutants). *Scf*$^{fl/-}$ mice were used as controls. +, WT allele; Δ, recombined *Scf*^{fl} allele; –, germline deleted allele. *Scf*$^{+/+}$ includes *Scf*$^{+/+}$, *Cre*(–); *Scf*$^{fl/+}$, *Pdgfrα-cre; Scf*$^{+/+}$, *Pdgfrα-cre; Scf*$^{fl/+}$, and *Cre*(–); *Scf*$^{fl/fl}$ mice. *Scf*$^{+/-}$ mice include *Pdgfra-cre; Scf*$^{+/-}$ and *Cre*(–); *Scf*$^{+/-}$ mice. All data represent mean ± SD. Two-tailed Student's t tests were used to evaluate statistical significance. *, P < 0.05.